POLITECNICO DI TORINO
Repository ISTITUZIONALE

The GaN Breakthrough for Sustainable and Cost-Effective Mobility Electrification and Digitalization

Original
The GaN Breakthrough for Sustainable and Cost-Effective Mobility Electrification and Digitalization / Scrimizzi, F., Cammarata, F., D'Agata, G., Nicolosi, G., Musumeci, S., Rizzo, S.A.. - In: ELECTRONICS. - ISSN 2079-9292. - ELETTRONICO. - 12:6(2023). [10.3390/electronics12061436]

Availability:
This version is available at: 11583/2980005 since: 2023-07-10T13:28:14Z

Publisher:
MDPI

Published
DOI:10.3390/electronics12061436

Terms of use:

This article is made available under terms and conditions as specified in the corresponding bibliographic description in the repository

Publisher copyright

(Article begins on next page)

28 June 2026

Available online at www.sciencedirect.com

ScienceDirect

Nuclear Physics B 893 (2015) 122–157

NUCLEAR PHYSICS B

www.elsevier.com/locate/nuclphysb

Decrypting $SO(10)$-inspired leptogenesis

Pasquale Di Bari [a,*], Luca Marzola [b,*], Michele Re Fiorentin [a,*]

[a] *Physics and Astronomy, University of Southampton, Southampton, SO17 1BJ, UK*
[b] *Institute of Physics, University of Tartu, Ravila 14c, 50411 Tartu, Estonia*

Received 20 December 2014; received in revised form 5 February 2015; accepted 6 February 2015

Available online 11 February 2015

Editor: Tommy Ohlsson

Abstract

Encouraged by the recent results from neutrino oscillation experiments, we perform an analytical study of $SO(10)$-inspired models and leptogenesis with hierarchical right-handed (RH) neutrino spectrum. Under the approximation of negligible misalignment between the neutrino Yukawa basis and the charged lepton basis, we find an analytical expression for the final asymmetry directly in terms of the low energy neutrino parameters that fully reproduces previous numerical results. This expression also shows that it is possible to identify an effective leptogenesis phase for these models. When we also impose the wash-out of a large pre-existing asymmetry $N_{B-L}^{\rm p,i}$, the strong thermal (ST) condition, we derive analytically all those constraints on the low energy neutrino parameters that characterise the ST-$SO(10)$-inspired leptogenesis solution, confirming previous numerical results. In particular we show why, though neutrino masses have to be necessarily normally ordered, the solution implies an analytical lower bound on the effective neutrinoless double beta decay neutrino mass, $m_{ee} \gtrsim 8$ meV, for $N_{B-L}^{\rm p,i} = 10^{-3}$, testable with next generation experiments. This, in combination with an upper bound on the atmospheric mixing angle, necessarily in the first octant, forces the lightest neutrino mass within a narrow range $m_1 \simeq$ (10–30) meV (corresponding to $\sum_i m_i \simeq$ (75–125) meV). We also show why the solution could correctly predict a non-vanishing reactor neutrino mixing angle and requires the Dirac phase to be in the fourth quadrant, implying $\sin\delta$ (and J_{CP}) negative as hinted by current global analyses. Many of the analytical results presented (expressions for the orthogonal matrix, RH neutrino mixing matrix, masses and phases) can have applications beyond leptogenesis.
© 2015 The Authors. Published by Elsevier B.V. This is an open access article under the CC BY license (http://creativecommons.org/licenses/by/4.0/). Funded by SCOAP[3].

* Corresponding authors.
E-mail addresses: pdb1d08@soton.ac.uk (P. Di Bari), luca.marzola@ut.ee (L. Marzola), mrf1g12@soton.ac.uk (M. Re Fiorentin).

http://dx.doi.org/10.1016/j.nuclphysb.2015.02.005
0550-3213/© 2015 The Authors. Published by Elsevier B.V. This is an open access article under the CC BY license (http://creativecommons.org/licenses/by/4.0/). Funded by SCOAP[3].

1. Introduction

There is no observational evidence of primordial antimatter in our observable Universe that, therefore, is matter–antimatter asymmetric. The matter–antimatter asymmetry can be expressed in terms of the baryon-to-photon number ratio, currently very precisely and accurately measured by the *Planck* satellite from CMB temperature anisotropies, finding [1]

$$\eta_B^{\rm CMB} = (6.1 \pm 0.1) \times 10^{-10} \,. \tag{1}$$

This value is too high to be explained within the Standard Model (SM) and, therefore, it can be regarded as an evidence of new physics. Leptogenesis [2] provides an attractive explanation since it is based on a minimal extension of the SM, the see-saw mechanism [3], able to address neutrino masses and mixing, soundly established by neutrino oscillation experiments. In this way leptogenesis realises a very interesting connection between two, apparently unrelated, fundamental physical observations: the cosmological matter–antimatter asymmetry and neutrino masses and mixing.

Recent important experimental findings support a traditional thermal picture and encourage further investigation in this direction. The confirmation of the BEH mechanism with the discovery of the Higgs boson at LHC, an important ingredient of the see-saw mechanism, certainly corroborates the overall picture of leptogenesis. In addition, the non-discovery of new physics at LHC so far, quite strongly constrains models of baryogenesis at the TeV (or lower) energy scale. Moreover if the recent claim of a B-mode polarisation signal in the CMB will be (even partially) confirmed (see [4] for critical analyses of BICEP2 results), it would support high inflationary scale $V^{1/4} \sim 10^{16}$ GeV [5]. In this way high values of the reheat temperature $T_{\rm RH}$, though not necessarily implied, would be not only possible but even quite natural. This phenomenological picture is then well compatible with the original idea of a high energy scale thermal leptogenesis scenario, much above the TeV scale [2].

Values of $T_{\rm RH}$ greater than those required by successful leptogenesis, $T_{\rm RH} \gtrsim 10^9$ GeV [6,7], would be not only possible but even, as already mentioned, quite natural if the BICEP2 signal, even just a small fraction of it, will be confirmed as primordial. In any case it is legitimate to conceive that other mechanisms of baryogenesis might have generated an asymmetry much larger than the observed one prior to the onset of leptogenesis, one of the three main working assumptions in our study. For example, considering that we will work within the context of $SO(10)$-inspired conditions (another of our main working assumptions), the decays of GUT gauge bosons might have acted as the source of such a large pre-existing asymmetry [8]. It is then quite legitimate to impose in addition to the successful leptogenesis condition, requiring that the asymmetry produced from right-handed (RH) neutrinos decays reproduces the observed asymmetry, that at the same time the RH neutrino inverse processes wash-out a possible pre-existing (too) large asymmetry generated by some external mechanism: we will refer to this condition as the ST (equilibrium) condition.[1]

Within a minimal type I extension of the SM and assuming a hierarchical RH neutrino mass spectrum, there is only one mass pattern able to realise successful ST leptogenesis, solving the

[1] This name is justified by the fact that, as we will discuss, because of flavour effects the washout of a pre-existing asymmetry is possible only locking all possible ways out in flavour space, i.e. imposing thermal equilibrium in all flavours, something that can be indeed regarded as a 'strong' thermal equilibrium condition. Note that it also ensures independence of the initial RH neutrino abundance.

problem of the initial conditions: the tauon N_2-dominated scenario [9].[2] In this scenario the lightest RH neutrino (N_1) mass has to be $M_1 \ll 10^9$ GeV so that the N_1 wash-out stage occurs in a three-flavoured regime [11,12]. This necessarily implies that the N_1-decays cannot produce a sizeable contribution to the final asymmetry [6,7]. On the other hand the next-to-lightest RH neutrino (N_2) mass falls in the range 10^{12} GeV $\gg M_2 \gg 10^9$ GeV so that the asymmetry production from N_2-decays occurs in the two-flavoured regime [11,12] and can be potentially sizeable. In this way the pre-existing large tauon asymmetry can be washed-out by the N_2-inverse processes while at the same time the N_2-decays can re-generate an asymmetry in the same tauon flavour. This tauon component would then explain the observed asymmetry if it can escape the N_1 wash-out. The latter, on the other hand, has necessarily to suppress the electron and muon pre-existing asymmetries since they cannot be fully washed-out by the N_2-inverse processes. This is because these can only wash-out the ℓ_2-flavour parallel component but not the orthogonal one, where ℓ_2 is the charged lepton flavour produced by N_2-decays [11,13].

It is quite interesting and non-trivial that so called $SO(10)$-inspired models [14–16] can indeed realise this seemingly contrived chain of conditions for successful ST leptogenesis [17]. This happens for a subset of the whole set of the solutions that realise successful $SO(10)$-inspired leptogenesis [18,19]. This subset defines the 'ST $SO(10)$-inspired solution' [17].

Interestingly, this solution implies a predictive set of constraints on low energy neutrino parameters that can be almost completely[3] tested by (data-taking or planned) low energy neutrino experiments (including cosmological observations). One of the most striking features is that the value of the absolute neutrino mass scale is quite constrained within a narrow window, such that the lightest neutrino mass $m_1 \simeq 20$ meV (corresponding to $\sum m_i \simeq 100$ meV). The Majorana phases are also constrained about particular values. In this way cancellations in the effective neutrino mass are very mild and $m_{ee} \sim 0.8\, m_1 \simeq 15$ meV. In addition parameters tested by neutrino oscillation experiments are also quite definitely predicted: neutrino masses have to be NO; the atmospheric mixing angle has to lie in the first octant and the Dirac phase in the fourth quadrant ($\delta \sim -\pi/4$) so that $\text{sign}(J_{CP}) = -\text{sign}(\eta_B) < 0$. It is also interesting that the solution has correctly predicted a non-vanishing value of the reactor mixing angle ($\theta_{13} \gtrsim 2°$–$3°$), as now robustly established by different experiments [20].[4]

This set of predictive constraints has so far been derived numerically, from scatter plots with points randomly generated [17]. A partial analytical insight was found for $SO(10)$-inspired solutions (no strong thermal condition) in the hierarchical limit [18], for $m_1 \ll 10$ meV, and, therefore, it does not apply to the strong thermal $SO(10)$-inspired solution that corresponds to semi-hierarchical (NO) neutrino masses. It has been recently shown analytically [22] that in general strong thermal leptogenesis requires, barring fine tuned models, $m_1 \gtrsim 10$ meV for NO. This is in complete agreement with the analogous lower bound found numerically in the case of the strong thermal $SO(10)$-inspired leptogenesis solution.

Encouraged by the recent experimental results, in addition to the above mentioned discovery of a non-vanishing reactor mixing angle also hints for negative values of J_{CP} [23,24] and, to a weaker extent, for a possible deviation of the atmospheric mixing angle from the maximal value

[2] This conclusion holds for hierarchical RH neutrino spectra, where wash-out and asymmetry production from each RH neutrino species occurs sequentially. It has been claimed that quasi-degenerate RH neutrino spectra might provide an alternative way to realise ST leptogenesis [9]. This claim seems to be supported by recent calculations within specific models [10].

[3] We will comment in the final discussion why 'almost'.

[4] Preliminary results were presented in [21].

[23,24] (see however [25]), in this paper we perform a systematic analytical derivation of the constraints coming from the strong thermal $SO(10)$-inspired solution confirming the numerical results. The derivation is made in the approximation $V_L \simeq I$, where V_L is the matrix describing the misalignment between the neutrino Yukawa basis and the charged lepton flavour basis but we also discuss the implications of small deviations at the level of the CKM quark mixing matrix.

The paper is organised as follows. In Section 2 we discuss the general set of conditions that lead to the solution. In Section 3 we discuss the current experimental results on neutrino parameters. In Section 4, imposing the $SO(10)$-inspired conditions, we derive compact analytic expressions for the RH neutrino mass spectrum and for the *CP* asymmetries improving and extending previous results [15,16,18]. In particular we are able to determine explicitly all the three phases associated to the eigenvalues of the Majorana mass matrix, an important ingredient to calculate correctly the *CP* asymmetries and, consequently, the final asymmetry. We also give an analytical expression for the orthogonal matrix that can be useful for model building considerations. In Section 5 we find an expression for the final asymmetry within $SO(10)$-inspired models in terms of the low energy neutrino parameters showing that it perfectly reproduces the numerical results for $V_L = I$: this represents one of the main results of our work. We then impose the successful leptogenesis condition and we find, for NO, a lower bound and an upper bound on m_1, an upper bound on the atmospheric mixing angle and different constraints on the low energy phases. In particular we show how $SO(10)$-inspired leptogenesis constraints are not symmetric under a change of the sign of J_{CP}, given by the sign of $\sin\delta$. In Section 6 we finally impose the ST condition and, still for NO, we show how the lightest neutrino mass is constrained within a narrow range and how a lower bound on the reactor mixing angle holds. We also show how this condition necessarily selects values of δ in the fourth quadrant. In Section 7 we discuss IO neutrino masses showing how in this case the ST condition cannot be satisfied and, therefore, this strictly implies NO neutrino masses. In Section 8 we make some final remarks on the different approximations and assumptions behind the results and on the testability of the solution in next years. In Section 9 we summarise our results.

2. Set of conditions: the general picture

The ST $SO(10)$-inspired leptogenesis solution is obtained imposing the following set of conditions on the see-saw parameter space:

(i) $SO(10)$-inspired conditions on the neutrino Dirac mass matrix;
(ii) successful leptogenesis;
(iii) strong thermal leptogenesis.

Let us briefly discuss these conditions in general, showing how (i) and (ii)+(iii) both independently select the N_2-dominated scenario and how (iii) specifies that the asymmetry has to be necessarily tauon dominated [9].

2.1. $SO(10)$-inspired conditions

In the minimal see-saw mechanism the SM Lagrangian is augmented introducing RH neutrinos with Yukawa couplings h and a Majorana mass term M. In the (flavour) basis, where

both charged leptons and Majorana mass matrices are diagonal, the leptonic mass terms after spontaneous symmetry breaking, can be written as ($\alpha = e, \mu, \tau$ and $i = 1, 2, 3$)

$$-\mathcal{L}_M = \overline{\alpha_L}\, D_{m_\ell}\, \alpha_R + \overline{\nu_{\alpha L}}\, m_{D\alpha i}\, N_{iR} + \frac{1}{2}\, \overline{N^c_{iR}}\, D_M\, N_{iR} + \text{h.c.}\,, \tag{2}$$

where $D_{m_\ell} \equiv \text{diag}(m_e, m_\mu, m_\tau)$ and $D_M \equiv \text{diag}(M_1, M_2, M_3)$, with $M_1 \leq M_2 \leq M_3$. The neutrino Dirac mass matrix m_D in the flavour basis can then be written in the bi-unitary parameterisation as

$$m_D = V_L^\dagger\, D_{m_D}\, U_R\,, \tag{3}$$

where $D_{m_D} \equiv \text{diag}(m_{D1}, m_{D2}, m_{D3})$ is the neutrino Dirac mass matrix in the Yukawa basis and V_L and U_R are the unitary matrices acting respectively on the LH and RH neutrino fields in the transformation from the flavour basis to the Yukawa basis.

If we parametrise the three eigenvalues in the Dirac mass matrix in terms of the up quark masses, writing

$$m_{D1} = \alpha_1\, m_u\,,\ m_{D2} = \alpha_2\, m_c\,,\ m_{D3} = \alpha_3\, m_t\,, \tag{4}$$

we define $SO(10)$-inspired models those respecting the following conditions[5]

(i) $I \leq V_L \lesssim V_{CKM}$,
(ii) $\alpha_i = \mathcal{O}(0.1\text{–}10)$.

With the condition (i) we mean that the values of the three mixing angles in V_L, that we indicate with $\theta^L_{12}, \theta^L_{13}, \theta^L_{23}$ in the usual PDG parametrisation, are not too larger than the corresponding mixing angles in the CKM matrix and in particular $\theta^L_{12} \lesssim \theta^{CKM}_{12} \equiv \theta_C \simeq 13^\circ$. In the see-saw limit, for $M \gg m_D$, the spectrum of neutrino mass eigenstates splits into a very heavy set, $N_i \simeq N_{iR} + N^c_{iR}$, with masses almost coinciding with the Majorana masses M_i, and into a light set $\nu_i \simeq \nu_{iL} + \nu^c_{iL}$, with a symmetric mass matrix m_ν given by the see-saw formula

$$m_\nu = -m_D\, \frac{1}{D_M}\, m_D^T\,. \tag{5}$$

[5] These conditions can be also satisfied beyond traditional $SO(10)$-models, see examples discussed in [26], the 5D-$SO(10)$ model [27], the 'tetra-model' [28] or the 'A to Z' model [29]. Vice-versa not all $SO(10)$-models necessarily respect them. For example they could give rise to a type II see-saw [30] contribution for the neutrino masses (e.g. [31]) and to alternative leptogenesis scenarios than those considered here. It should also be said that traditional (4D, no flavour symmetries) $SO(10)$ models that have been explored as viable realistic models able to fit both quarks and leptons parameters also usually respect these conditions (see discussion in [18]). For example if we consider a recent result of a best fit within a non-supersymmetric $SO(10)$ model using 126 and 10-dim Higgs representations including RG corrections [32] we obtain: $(\alpha_1, \alpha_2, \alpha_3, \theta^L_{12}, \theta^L_{13}, \theta^L_{23}) \simeq (48, 8, 1, 1^\circ, 3^\circ, 4^\circ)$. The large value of α_1 lifts M_1. Away from the crossing level solution, where $M_1 \simeq M_2$, one still has $M_1 \lesssim 10^9$ GeV. The best fit hits precisely a crossing level solution at $m_1 \simeq 2$ meV (signalled by the low value of $m_{ee} \ll 1$ meV). This probably happens since the crossing level allows the largest possible value for θ_{23}. This is found to be $\theta_{23} \sim 36^\circ$, a value 3σ below the best experimental fit (explaining the quite high value $\chi^2_{\text{min}} \sim 10$). In addition the Dirac phase is found $\delta \simeq 0$ and neutrino masses are NO. The latest neutrino data increase the tension, since values $\theta_{23} \sim 36^\circ$ are even more strongly disfavoured (cf. Eq. (13)) and values $\delta \sim 0$ are now also disfavoured at $\sim 2\sigma$ (cf. Eq. (14)). A more promising case seems to be a supersymmetric $SO(10)$ model also including a 120_H. This time the best fit is found for IO and we find that also in this case the model respects the $SO(10)$-inspired conditions (one has $(\alpha_1, \alpha_2, \alpha_3, \theta^L_{12}, \theta^L_{13}, \theta^L_{23}) \simeq (0.3, 6, 0.5, 4^\circ, 0.2^\circ, 13^\circ)$). Because of the small value of α_1 one finds $M_1 \sim 1$ TeV. Our calculations can be easily extended to treat also this supersymmetric case [33].

This is diagonalised by a unitary matrix U,

$$U^\dagger m_\nu U^\star = -D_m \,, \tag{6}$$

where $D_m \equiv \mathrm{diag}(m_1, m_2, m_3)$ with $m_1 \leq m_2 \leq m_3$, corresponding to the PMNS leptonic mixing matrix, in a way that we can write

$$D_m = U^\dagger m_D \frac{1}{D_M} m_D^T U^\star \,. \tag{7}$$

When the current experimental information from neutrino oscillation experiments on the leptonic mixing matrix and on the neutrino masses is taken into account, the RH neutrino mass spectrum, barring regions around crossing level solutions [16], turns out to be highly hierarchical with approximately $M_1 : M_2 : M_3 = \alpha_1^2 m_u^2 : \alpha_2^2 m_c^2 : \alpha_3^2 m_t^2$, implying $M_1 \ll 10^9$ GeV, 10^9 GeV $\lesssim M_2 \lesssim 10^{12}$ GeV and $M_3 \gg 10^{12}$ GeV.[6] In this way the lightest RH neutrino is too light to contribute significantly to the final asymmetry when successful leptogenesis is imposed. The heaviest RH neutrino also gives vanishing or in any case negligible contribution, since either it is not thermalised at all or, even if it is thermalised, its total *CP* asymmetry is strongly suppressed. In this situation the only RH neutrino species that can give a sizeable asymmetry able to explain the observed one is N_2 and in this way, the $SO(10)$-inspired conditions naturally realise the N_2-dominated scenario [35]. This is crucially possible thanks to flavour effects [11,12] that enlarge the regions where the lightest RH neutrino wash-out is negligible and the N_2-asymmetry can survive [36,37].

In addition to a strong hierarchy of the mass spectrum, in the approximation $V_L \simeq I$, the N_2-flavoured *CP* asymmetries are also strongly hierarchical with $\varepsilon_{2\tau} \gg \varepsilon_{2\mu} \gg \varepsilon_{2e}$ and this results into a tauon dominated final asymmetry [18]. Relaxing the approximation $V_L \simeq I$ this conclusion partially changes since a muon-dominated type solution becomes also possible. This, however, exists only for large values of the lightest neutrino mass $m_1 \gtrsim 0.01$ eV so that it is fair to say that $SO(10)$-inspired conditions typically imply a tauon N_2-dominated scenario. In the next section we will discuss this result in detail.

2.2. Successful ST leptogenesis

Let us now shortly discuss the two conditions imposed by leptogenesis, successful and ST leptogenesis conditions. It is convenient to discuss them separately, in a way to highlight more clearly the different steps leading to the tauon N_2-dominated scenario as the only way to realise successful ST leptogenesis. For illustrative purposes it is convenient to start from the ST condition.

2.2.1. ST leptogenesis condition

Since we are assuming a hierarchical RH neutrino mass spectrum, with $M_3 \gtrsim 3\, M_2$ and $M_2 \gtrsim 3\, M_1$, the decays and wash-out processes associated to each RH neutrino species occur sequentially, with no overlap [38]. In this situation a pre-existing asymmetry, while temperature drops down in the expanding very early Universe, undergoes a multiple stage wash-out, involving sequentially each RH neutrino species, starting from the N_3-washout stage (if N_3 is thermalised) and ending with the N_1-washout stage.

[6] For recent models realising crossing level solutions, where either two or all three RH neutrino masses are quasi-degenerate and *CP* asymmetries are enhanced, see [34].

However, since in the one-flavoured regime (for $M_i \gtrsim 10^{12}$ GeV) each RH neutrino species is able to wash-out only a component of the asymmetry in a flavour space direction $\ell_i \propto (|m_{Dei}|^2, |m_{D\mu i}|^2, |m_{D\tau i}|^2)$ [11] and since, in general the three flavour directions (ℓ_1, ℓ_2, ℓ_3) do not form an orthonormal basis,[7] for simple geometric reasons the only possibility to fully wash-out a generic pre-existing asymmetry is that (at least) the N_1 wash-out stage occurs in the three flavoured regime [13]. In this case the most straightforward way to realise ST leptogenesis would be to impose strong N_1 wash-out in each flavour. This condition can be expressed as $K_{1\alpha} \gg 1$, having defined, for any $\alpha = e, \mu, \tau$, the flavour decay parameters

$$K_{i\alpha} \equiv \frac{\Gamma_{i\alpha} + \overline{\Gamma}_{i\alpha}}{H(T = M_i)} = \frac{|m_{D\alpha i}|^2}{M_i\, m_\star}\,, \tag{8}$$

where $\Gamma_{i\alpha} = \Gamma(N_i \to \phi^\dagger l_\alpha)$ and $\bar{\Gamma}_{i\alpha} = \Gamma(N_i \to \phi\, \bar{l}_\alpha)$ are the zero temperature limit of the flavoured decay rates into α leptons and anti-leptons in the three-flavoured regime and $m_\star \simeq 1.1 \times 10^{-3}$ eV is the equilibrium neutrino mass. This simple set of conditions is, however, too restrictive to allow also successful leptogenesis, since the lightest RH neutrino washout would act strongly not only on all components of the pre-existing asymmetry but also on the leptogenesis contribution from N_2-decays.[8]

2.2.2. Successful leptogenesis condition

The only way to realise successful ST leptogenesis is to have the wash-out of the pre-existing asymmetry occurring in two separate steps. In a first step, imposing $K_{2\tau} \gg 1$, the tauon component of the pre-existing asymmetry is N_2 washed-out in the two-flavoured regime, implying 10^9 GeV $\ll M_2 \ll 10^{12}$ GeV. In the second step the N_1-washout stage has still to occur in the three flavoured regime ($M_1 \ll 10^9$ GeV) in a way that, imposing $K_{1e}, K_{1\mu} \gg 1$, it can eventually suppress also the electron and muon components of the pre-existing asymmetries. This time, however, the tauon asymmetry generated by the N_2-decays at the end of the N_2 washout stage, the genuine contribution from leptogenesis, can be sufficiently large to explain the observed asymmetry if at the same time the N_1 wash-out in the tauon flavour is weak, i.e. if $K_{1\tau} \lesssim 1$. In this way the successful ST leptogenesis necessarily leads to a tauon N_2-dominated scenario, where the final asymmetry is dominated by the tauon flavour component produced by the out-of-equilibrium N_2-decays.

It is quite interesting, and highly non-trivial, that $SO(10)$-inspired models naturally realise this kind of leptogenesis scenario and can, therefore, also potentially realise successful ST leptogenesis. However, as we have seen, successful ST leptogenesis also requires the additional conditions

$$K_{1e}, K_{1\mu}, K_{2\tau} \gg 1\,, \tag{9}$$

and it is then to be verified whether these can be met within $SO(10)$-inspired models.

Summarising, we have a situation where both $SO(10)$-inspired and successful strong thermal leptogenesis might be simultaneously realised for an interesting (intersection) region in the space of see-saw parameters. If this region exists, then it is clearly very interesting to understand

[7] On the other hand if they would form an orthonormal basis, there would be no interference among the RH neutrinos and successful leptogenesis would be simply impossible since all *CP* asymmetries would vanish [39].

[8] On the other hand this set up might be useful to have the wash-out of a pre-existing $B - L$ asymmetry in some baryogenesis model, e.g. electroweak baryogenesis, occurring at some energy scale lower than the N_1 wash-out.

what are the corresponding constrains on the low energy neutrino parameters. In the following discussion, our main objective will be to show analytically not only that such region exists, confirming the numerical results [17], but also that it indeed implies definite constraints on the low energy neutrino parameters if the pre-existing $B-L$ asymmetry is sufficiently large. We will derive these constraints in the approximation $V_L \simeq I$. Finally we will compare the analytical results with the numerical results obtained in [17] and also discuss how the constraints get slightly relaxed going beyond the approximation $V_L \simeq I$.

3. Low energy neutrino data

As we will see the final asymmetry from $SO(10)$-inspired leptogenesis depends in such a non-trivial way on low energy neutrino parameters that the successful leptogenesis conditions strongly links them, in a way that any experimental information on one parameter usually produces constraints also on the other parameters. The main goal is to be able to place constraints that can be tested by future experiments. In this section we briefly review the current experimental information on low energy neutrino parameters that we will employ for the derivation of the constraints.

Neutrino oscillation experiments measure two mass squared differences, $\Delta m^2_{\rm atm}$ and $\Delta m^2_{\rm sol}$. Neutrino masses can then be either NO, with $m_2^2 - m_1^2 = \Delta m^2_{\rm sol}$ and $m_3^2 - m_2^2 = \Delta m^2_{\rm atm}$, or IO, with $m_3^2 - m_2^2 = \Delta m^2_{\rm sol}$ and $m_2^2 - m_1^2 = \Delta m^2_{\rm atm}$. For example, in a recent global analysis [24] it is found $m_{\rm atm} \equiv \sqrt{m_3^2 - m_1^2} \simeq 0.0495$ eV and $m_{\rm sol} \equiv \sqrt{\Delta m^2_{\rm sol}} \simeq 0.0087$ eV.

Finally, the cosmological observations place an upper bound on the sum of the neutrino masses and recently the Planck Collaboration found $\sum_i m_i \lesssim 0.23$ [1] eV that, combined with the measurements of $m_{\rm sol}$ and $m_{\rm atm}$, translates into the upper bound

$$m_1 \lesssim 0.07 \text{ eV} . \tag{10}$$

For NO the leptonic mixing matrix can be parameterised in the usual standard way[9]

$$U^{(\rm NO)} = \begin{pmatrix} c_{12}\, c_{13} & s_{12}\, c_{13} & s_{13}\, e^{-{\rm i}\,\delta} \\ -s_{12}\, c_{23} - c_{12}\, s_{23}\, s_{13}\, e^{{\rm i}\,\delta} & c_{12}\, c_{23} - s_{12}\, s_{23}\, s_{13}\, e^{{\rm i}\,\delta} & s_{23}\, c_{13} \\ s_{12}\, s_{23} - c_{12}\, c_{23}\, s_{13}\, e^{{\rm i}\,\delta} & -c_{12}\, s_{23} - s_{12}\, c_{23}\, s_{13}\, e^{{\rm i}\,\delta} & c_{23}\, c_{13} \end{pmatrix} \times {\rm diag}\left(e^{i\,\rho}, 1, e^{i\,\sigma}\right) , \tag{11}$$

($s_{ij} \equiv \sin\theta_{ij}, c_{ij} \equiv \cos\theta_{ij}$) while for IO, within our labelling convention for light neutrino masses and adopting the usual definition for the thee mixing angles θ_{ij}, the columns of the leptonic mixing matrix have to be permuted in a way that

$$U^{(\rm IO)} = \begin{pmatrix} s_{13}\, e^{-{\rm i}\,\delta} & c_{12}\, c_{13} & s_{12}\, c_{13} \\ s_{23}\, c_{13} & -s_{12}\, c_{23} - c_{12}\, s_{23}\, s_{13}\, e^{{\rm i}\,\delta} & c_{12}\, c_{23} - s_{12}\, s_{23}\, s_{13}\, e^{{\rm i}\,\delta} \\ c_{23}\, c_{13} & s_{12}\, s_{23} - c_{12}\, c_{23}\, s_{13}\, e^{{\rm i}\,\delta} & -c_{12}\, s_{23} - s_{12}\, c_{23}\, s_{13}\, e^{{\rm i}\,\delta} \end{pmatrix} \times {\rm diag}\left(e^{i\,\sigma}, e^{i\,\rho}, 1\right) . \tag{12}$$

[9] In the PDG parameterisation the matrix of Majorana phases is defined as ${\rm diag}\left(1, e^{i\,\frac{\alpha_{21}}{2}}, e^{i\,\frac{\alpha_{31}}{2}}\right)$ and, therefore, one simply has $\alpha_{31} = 2(\sigma - \rho)$ and $\alpha_{21} = -2\,\rho$.

The mixing angles, respectively the reactor, the solar and the atmospheric ones, are now measured with the following best fit values and 1σ (3σ) ranges [23] for NO and IO respectively,

$$\begin{aligned}
&\theta_{13} = 8.8^\circ \pm 0.4^\circ \;\; (7.6^\circ\text{–}9.9^\circ) \;\text{ and }\; \theta_{13} = 8.9^\circ \pm 0.4^\circ \;\; (7.7^\circ\text{–}9.9^\circ)\,,\\
&\theta_{12} = 33.7^\circ \pm 1.1^\circ \;\; (30.6^\circ\text{–}36.8^\circ) \;\text{ and }\; \theta_{12} = 33.7^\circ \pm 1.1^\circ \;\; (30.6^\circ\text{–}36.8^\circ)\,,\\
&\theta_{23} = 41.4^\circ{}^{+1.9^\circ}_{-1.4^\circ} \;\; (37.7^\circ\text{–}52.3^\circ) \;\text{ and }\; \theta_{23} = 42.4^\circ{}^{+8.0^\circ}_{-1.8^\circ} \;\; (38.1^\circ\text{–}52.3^\circ)\,.
\end{aligned} \tag{13}$$

It is interesting that current experimental data also start to put constraints on the Dirac phase and the following best fit values and 1σ errors are found for NO and IO respectively,

$$\delta/\pi = -0.61^{+0.38}_{-0.27} \;\text{ and }\; \delta/\pi = -0.69^{+0.29}_{-0.33}\,, \tag{14}$$

while all values $[-\pi, +\pi]$ are still allowed at $3\,\sigma$.

4. From *SO*(10)-inspired conditions to RH neutrino masses and *CP* flavoured asymmetries

In this section we show how the $SO(10)$-inspired conditions imply, in the hierarchical case, an N_2-dominated RH neutrino mass spectrum [15]. Only for particular conditions on the low energy neutrino parameters, there exist crossing level solutions, in vicinity of which two or even all three RH neutrino masses are quasi-degenerate [16]. We derive compact analytic expressions both for the RH neutrino masses and for their *CP* asymmetries and compare them with the numerical results for some selected examples.

4.1. RH neutrino masses

Inserting the bi-unitary parameterisation Eq. (3) into the diagonalised see-saw formula Eq. (7) one obtains an expression for the (symmetric) inverse Majorana mass matrix in the Yukawa basis, $M^{-1} = U_R\, D_M^{-1}\, U_R^T$, in terms of the unitary matrix V_L, the low energy neutrino mass matrix $m_\nu = -U\, D_m\, U^T$ and the three neutrino Yukawa eigenvalues m_{Di},

$$M^{-1} = D_{m_D}^{-1}\, V_L\, U\, D_m\, U^T\, V_L^T\, D_{m_D}^{-1}\,. \tag{15}$$

This can be also easily inverted obtaining for the Majorana mass matrix in the Yukawa basis, $M = U_R^\star\, D_M\, U_R^\dagger$,

$$M = D_{m_D}\, V_L^\star\, U^\star\, D_m^{-1}\, U^\dagger\, V_L^\dagger\, D_{m_D}\,. \tag{16}$$

From these expressions, either from M^{-1} or from M, one can derive the RH neutrino mass spectrum and the RH neutrino mixing matrix U_R, as a function of the 9 low energy neutrino parameters in m_ν (6 mixing parameters in U and 3 light neutrino masses m_i), the 6 parameters in the unitary matrix V_L and the 3 Dirac neutrino masses m_{Di}.

This can be done diagonalising the hermitian matrix $M^\dagger M = U_R\, D_M^2\, U_R^\dagger$ (or equivalently $M^{-1}\,(M^{-1})^\dagger = U_R\, D_M^{-2}\, U_R^\dagger$). For a given U_R, any matrix $\widetilde{U}_R = U_R\, D_\phi^{-1}$, where

$$D_\phi \equiv (e^{-i\,\frac{\Phi_1}{2}}, e^{-i\,\frac{\Phi_2}{2}}, e^{-i\,\frac{\Phi_3}{2}}) \tag{17}$$

is a generic diagonal unitary matrix, also diagonalises M and M^{-1}. However, going back to the (Takagi) diagonalisation $M = U_R^\star\, D_M\, U_R^\dagger$ and given a $\widetilde{U}_R$, one can unambiguously fix [19]

$$D_\phi = \sqrt{D_M\, \widetilde{U}_R^\dagger\, M^{-1}\, \widetilde{U}_R^\star}\,. \tag{18}$$

If one is not in the vicinity of crossing level solutions, where at least two RH neutrino masses become degenerate, the RH neutrino mass spectrum is strongly hierarchical and analytical expressions can be easily found [15,16]. Here we adopt a slightly different procedure that yields simplified and more compact expressions in terms both of the light neutrino mass and of the inverse light neutrino mass matrix entries. If we start from Eq. (16) for M, in the approximation $V_L \simeq I$, we can write

$$U_R^\star \, D_M \, U_R^\dagger \simeq D_{m_D} \, U^\star \, D_m^{-1} \, U^\dagger \, D_{m_D} \, . \tag{19}$$

Considering that from the definition of U (cf. Eq. (6)) one easily finds

$$m_\nu^{-1} = -U^\star \, D_m^{-1} \, U^\dagger \, , \tag{20}$$

Eq. (19) can be also written more compactly as

$$M = U_R^\star \, D_M \, U_R^\dagger \simeq -D_{m_D} \, m_\nu^{-1} \, D_{m_D} \, . \tag{21}$$

This equation shows that $M_{i3}/M_{33} = M_{3i}/M_{33} \propto m_{Di}/m_{D3}$ and, therefore, in first approximation the LH side is in a block diagonal form and, neglecting terms $\mathcal{O}(m_{D1}/m_{D3}, m_{D2}/m_{D3})$ one finds

$$M_3 \simeq m_{D3}^2 \, |(m_\nu^{-1})_{\tau\tau}| = m_{D3}^2 \left| \frac{(U_{\tau 1}^\star)^2}{m_1} + \frac{(U_{\tau 2}^\star)^2}{m_2} + \frac{(U_{\tau 3}^\star)^2}{m_3} \right| \propto \alpha_3^2 \, m_t^2 \, . \tag{22}$$

At the same time the phase Φ_3 is also specified and one simply has

$$\Phi_3 = \mathrm{Arg}[-(m_\nu^{-1})_{\tau\tau}] \, . \tag{23}$$

The same procedure can be adopted for M^{-1}, rewriting Eq. (15) in the approximation $V_L \simeq I$ and imposing the Takagi diagonalisation

$$M^{-1} = U_R \, D_M^{-1} \, U_R^T \simeq D_{m_D}^{-1} \, U \, D_m \, U^T \, D_{m_D}^{-1} = -D_{m_D}^{-1} \, m_\nu \, D_{m_D}^{-1} \, . \tag{24}$$

This time the RH side is approximately in a block-diagonal form with $M_{i1}^{-1}/M_{11}^{-1} = M_{1i}^{-1}/M_{11}^{-1} \propto m_{D1}/m_{Di}$, so that the largest M^{-1} eigenvalue, $1/M_1$, can be written as $1/M_1 \simeq |m_{vee}|/m_{D11}^2$ and, therefore,

$$M_1 \simeq \frac{m_{D1}^2}{|m_{vee}|} = \frac{m_{D1}^2}{|m_1 \, U_{e1}^2 + m_2 \, U_{e2}^2 + m_3 \, U_{e3}^2|} \propto \alpha_1^2 \, m_u^2 \, . \tag{25}$$

Also in this case the procedure allows to specify the phase Φ_1,

$$\Phi_1 = \mathrm{Arg}[-m_{vee}^\star] \, . \tag{26}$$

Finally, from the approximate expressions Eq. (22) for M_3 and Eq. (25) for M_1, one can also easily find an approximate expression for M_2. From the see-saw formula Eq. (7) one has

$$m_1 \, m_2 \, m_3 = \frac{m_{D1}^2 \, m_{D2}^2 \, m_{D3}^2}{M_1 \, M_2 \, M_3} \, e^{i \, (2 \, \widetilde{\Phi}_R - 2 \, \Phi_U - \sum_i \, \Phi_i)} \, , \tag{27}$$

where $\widetilde{\Phi}_R \equiv \mathrm{Arg}[\det(\widetilde{U}_R)]$ and $\Phi_U \equiv \mathrm{Arg}[\det(U)] = \rho + \sigma$, implying $\sum_i \Phi_i = 2\,(\widetilde{\Phi}_R - \Phi_U)$. In this way we can write

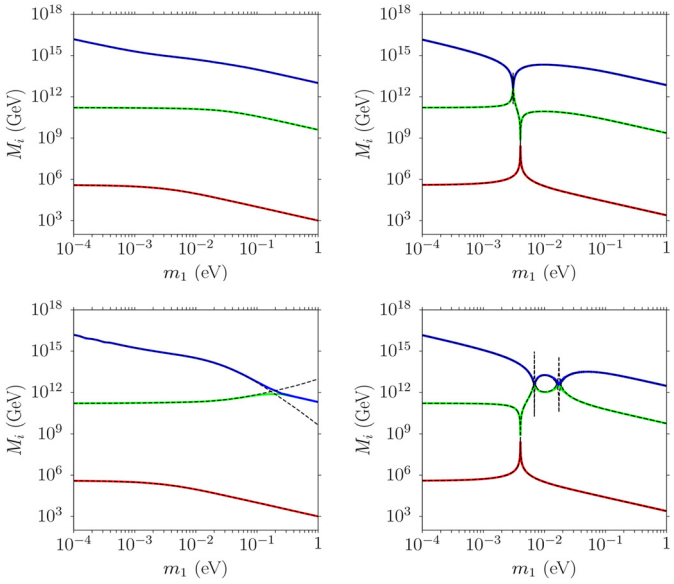

Fig. 1. Comparison between the numerical solutions for the RH neutrino masses (solid lines) and the analytical solutions Eqs. (22), (28) and (25) (dashed lines). The solutions are obtained for $\theta_{13} = 0$, $\theta_{23} = 45°$, $\theta_{12} = 33°$, $\alpha_1 = \alpha_2 = \alpha_3 = 1$, $V_L = I$ and for $(\rho, \sigma) = (0, 0), (\pi/2, 0), (0, \pi/2), (\pi/2, \pi/2)$ from top left to bottom right respectively.

$$M_2 \simeq \frac{m_{D2}^2}{m_1\, m_2\, m_3}\, \frac{|m_{vee}|}{|(m_\nu^{-1})_{\tau\tau}|} = m_{D2}^2\, \frac{|m_1\, U_{e1}^2 + m_2\, U_{e2}^2 + m_3\, U_{e3}^2|}{|m_2\, m_3\, U_{\tau 1}^{\star 2} + m_1\, m_3\, U_{\tau 2}^{\star 2} + m_1\, m_2\, U_{\tau 3}^{\star 2}|}$$
$$\propto \alpha_2^2\, m_c^2\,, \tag{28}$$

and for the phase $\Phi_2 = 2\,(\widetilde{\Phi}_R - \Phi_U) - \Phi_3 - \Phi_1$ one finds

$$\Phi_2 = \mathrm{Arg}\left[\frac{m_{vee}}{(m_\nu^{-1})_{\tau\tau}}\right] + 2\,\widetilde{\Phi}_R - 2\,(\rho + \sigma)\,. \tag{29}$$

It is easy to see from the above general expressions, that in the hierarchical limit, $m_1 \ll m_{\rm sol}$ (remember that we are assuming NO), the RH neutrino masses tend to the following simple expressions [15,16]

$$M_1 \simeq \frac{m_{D1}^2}{|m_{\rm sol}\, s_{12}^2\, c_{13}^2 + m_{\rm atm}\, s_{13}^2\, e^{i\,(2\,\sigma - \delta)}|} \approx \frac{m_{D1}^2}{m_{\rm sol}\, s_{12}^2}\,,$$
$$M_2 \simeq \frac{m_{D2}^2\, |m_{\rm sol}\, s_{12}^2\, c_{13}^2 + m_{\rm atm}\, s_{13}^2\, e^{i\,(2\,\sigma - \delta)}|}{m_{\rm sol}\, m_{\rm atm}\, |s_{12}\, s_{23} - c_{12}\, c_{23}\, s_{13}\, e^{-i\,\delta}|^2} \approx \frac{m_{D2}^2}{m_{\rm atm}\, s_{23}^2}\,,$$
$$M_3 \simeq \frac{m_{D3}^2\, |s_{12}\, s_{23} - c_{12}\, c_{23}\, s_{13}\, e^{-i\,\delta}|^2}{m_1} \approx \frac{m_{D3}^2}{m_1}\, s_{12}^2\, s_{23}^2\,, \tag{30}$$

where the last ones are obtained within the (rough) approximation $s_{13} \simeq 0$. In Fig. 1 we compare the found approximated analytic expressions for the RH neutrino masses (cf. Eqs. (22), (25) and (28)) with the numerical solutions for the simple four sets of parameters yielding level crossings for special values of m_1 as discussed in [16] (note that for simplicity $\theta_{13} = 0$

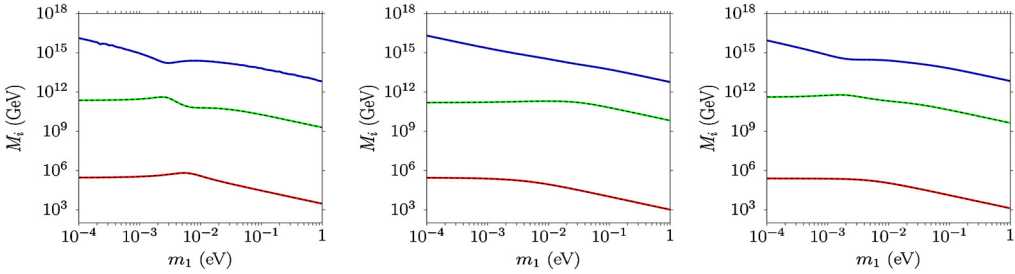

Fig. 2. Comparison of the analytical expressions for the RH neutrino masses (cf. Eqs. (22), (28), (25), dashed lines) with the numerical solutions (solid lines) versus m_1 for the three following sets of parameters: $V_L = I$, $(\alpha_1, \alpha_2, \alpha_3) = (1, 5, 1)$, $\theta_{13} = (7.55°, 8.14°, 9.2°)$, $\theta_{12} = (35.2°, 34.75°, 35.0°)$, $\theta_{23} = (46.2°, 42.1°, 40.0°)$, $\delta/\pi = (0.275, 0.067, -0.24)$, $\rho/\pi = (0.54, 1.080, 0.24)$, $\sigma/\pi = (1.14, 0.94, 0.80)$. These three solutions are examples of τ_A, τ_B and strong thermal solutions respectively and realise successful leptogenesis for $m_1 \simeq (2.5, 300, 10)$ meV. All three cases are for NO. (For interpretation of the references to colour in this figure, the reader is referred to the web version of this article.)

and $\theta_{23} = \pi/4$). For the up quark masses at the leptogenesis scale,[10] we adopted the values $(m_u, m_c, m_t) = (1\text{ MeV}, 400\text{ MeV}, 100\text{ GeV})$ [40]. It can be noticed how the analytic solutions (dashed black lines) track perfectly the numerical ones (solid coloured lines) except in the close vicinity of those values of m_1 where the RH neutrino masses become quasi-degenerate and the validity of the adopted approximations breaks down. In the panels of Fig. 2 we show the same comparison but this time with three solutions realising successful (non-resonant) $SO(10)$-inspired leptogenesis, around some (indicated) values of m_1 for NO. The first two cases realise two different types of tauon N_2-dominated leptogenesis solutions so called type A and type B [18,19] that we will fully describe analytically in Section 5. The third case is a strong thermal $SO(10)$-inspired solution [18,19] (realised for $m_1 \simeq 10$ meV and $N^{\rm p,i}_{B-L} = 0.001$). As we will discuss in Section 6, this can only emerge within type A solutions. As one can see this time there are no level crossings and the analytic solutions perfectly track the numerical ones for any value of m_1. These results show explicitly how we can safely adopt the analytic solutions in our following discussion, though it should be made clear that the comparison is made for $V_L = I$ and, therefore, at this stage we are not testing the validity of the approximation $V_L \simeq I$ that will instead be discussed in Section 8.1.

It is also possible to find an analytical approximate expression for the RH neutrino mixing matrix U_R. From the discussion above it should be clear that U_R is of the form $U_R = I + \xi$, where $\xi_{ii} = 0$ and the $\xi_{i\neq j}$ leading terms are suppressed $\propto m_{Di}/m_{Dj}$ with $j > i$ in a way that U_R is well approximated by

$$U_R \simeq \begin{pmatrix} 1 & -\frac{m_{D1}}{m_{D2}}\frac{m^\star_{ve\mu}}{m^\star_{vee}} & \frac{m_{D1}}{m_{D3}}\frac{(m_\nu^{-1})^\star_{e\tau}}{(m_\nu^{-1})^\star_{\tau\tau}} \\ \frac{m_{D1}}{m_{D2}}\frac{m_{ve\mu}}{m_{vee}} & 1 & \frac{m_{D2}}{m_{D3}}\frac{(m_\nu^{-1})^\star_{\mu\tau}}{(m_\nu^{-1})^\star_{\tau\tau}} \\ \frac{m_{D1}}{m_{D3}}\frac{m_{ve\tau}}{m_{vee}} & -\frac{m_{D2}}{m_{D3}}\frac{(m_\nu^{-1})_{\mu\tau}}{(m_\nu^{-1})_{\tau\tau}} & 1 \end{pmatrix} D_\Phi, \tag{31}$$

equivalent to the expression in [16] but where we identified neutrino mass matrices combinations with entries of the inverse neutrino mass matrix, something that will prove very useful when we

[10] In the case of $SO(10)$-inspired models this is approximately given by $T_L \sim (3\text{–}10) \times 10^{10}$ GeV as we will show later.

will extract the constraints on the low energy neutrino parameters. Details on the derivation can be found in Appendix A. It should be noticed that the phases Φ_i are now specialised in a way that $\widetilde{\Phi}_R \simeq 0$, so that Eq. (29) for Φ_2 becomes

$$\Phi_2 = \text{Arg}\left[\frac{m_{vee}}{(m_\nu^{-1})_{\tau\tau}}\right] - 2\,(\rho+\sigma)\,. \tag{32}$$

It can be also useful to calculate the orthogonal matrix Ω within $SO(10)$-inspired models. Starting from the orthogonal parameterisation for the neutrino Dirac mass matrix in the charged lepton basis [41], $m_D = U\sqrt{D_m}\,\Omega\,\sqrt{D_M}$ where $\Omega\,\Omega^T = I$, and comparing with the bi-unitary parameterisation Eq. (3), one finds straightforwardly an expression for the orthogonal parameterisation [18] $\Omega = D_m^{-\frac{1}{2}}\,U^\dagger\,V_L^\dagger\,D_{m_D}\,U_R\,D_M^{-\frac{1}{2}}$, that in the approximation $V_L \simeq I$ simplifies into $\Omega \simeq D_m^{-\frac{1}{2}}\,U^\dagger\,D_{m_D}\,U_R\,D_M^{-\frac{1}{2}}$, that in term of the entries can be written as

$$\Omega_{ij} \simeq \frac{1}{\sqrt{m_i\,M_j}}\sum_k m_{Dk}\,U^\star_{ki}\,U_{Rkj}\,. \tag{33}$$

From Eq. (31) one can then find this approximate expression for Ω (see Appendix A),

$$\Omega \simeq \begin{pmatrix} -\frac{\sqrt{m_1\,|m_{vee}|}}{m_{vee}}\,U_{e1} & \sqrt{\frac{m_2\,m_3\,|(m_\nu^{-1})_{\tau\tau}|}{|m_{vee}|}}\left(U^\star_{\mu 1} - U^\star_{\tau 1}\,\frac{(m_\nu^{-1})_{\mu\tau}}{(m_\nu^{-1})_{\tau\tau}}\right) & \frac{U^\star_{31}}{\sqrt{m_1\,|(m_\nu^{-1})_{\tau\tau}|}} \\ -\frac{\sqrt{m_2\,|m_{vee}|}}{m_{vee}}\,U_{e2} & \sqrt{\frac{m_1\,m_3\,|(m_\nu^{-1})_{\tau\tau}|}{|m_{vee}|}}\left(U^\star_{\mu 2} - U^\star_{\tau 2}\,\frac{(m_\nu^{-1})_{\mu\tau}}{(m_\nu^{-1})_{\tau\tau}}\right) & \frac{U^\star_{32}}{\sqrt{m_2\,|(m_\nu^{-1})_{\tau\tau}|}} \\ -\frac{\sqrt{m_3\,|m_{vee}|}}{m_{vee}}\,U_{e3} & \sqrt{\frac{m_1\,m_2\,|(m_\nu^{-1})_{\tau\tau}|}{|m_{vee}|}}\left(U^\star_{\mu 3} - U^\star_{\tau 3}\,\frac{(m_\nu^{-1})_{\mu\tau}}{(m_\nu^{-1})_{\tau\tau}}\right) & \frac{U^\star_{33}}{\sqrt{m_3\,|(m_\nu^{-1})_{\tau\tau}|}} \end{pmatrix} D_\Phi\,, \tag{34}$$

that in the limit $m_1 \to 0$ correctly reduces to the two RH neutrino limit form [42]

$$\Omega \xrightarrow{m_1\to 0} \begin{pmatrix} 0 & 0 & 1 \\ 1+\mathcal{O}(\theta_{13}) & \mathcal{O}(\theta_{13}) & 0 \\ \mathcal{O}(\theta_{13}) & 1+\mathcal{O}(\theta_{13}) & 0 \end{pmatrix}. \tag{35}$$

As we said in the introduction, and clearly shown in the examples of Fig. 2, barring regions around crossing level solutions, the $SO(10)$-inspired RH neutrino mass spectrum naturally realises the N_2-dominated scenario. This is because N_1 is too light to produce a sizeable asymmetry. At the same time, since $M_3 \gg 10^{12}$ GeV and the N_3 total asymmetry is strongly suppressed as $\varepsilon_3 \propto (M_2/M_3)^2$, the N_3-decays contribution to the final asymmetry is also negligible. In this way the only possibility to reproduce the final asymmetry relies on the N_2-production that occurs in the two-flavoured regime since $M_2 \sim 10^{10-11}$ GeV.

In the N_2-dominated scenario the contribution to the asymmetry from leptogenesis can be calculated as the sum of the three (charged lepton) flavoured asymmetries $\Delta_\alpha \equiv B/3 - L_\alpha$. Normalising the abundance N_X of a generic quantity X in a way that in the ultra-relativistic thermal equilibrium the abundance of RH neutrinos $N_{N_i}^{\text{eq}}(T \gg M_1) = 1$, the final asymmetry produced by the decays of the (N_2) RH neutrinos can then be written, in terms of the CP asymmetries $\varepsilon_{2\alpha}$ and the efficiency factors $\kappa(K_{2\alpha})$ at the production, as [36,37,43,39]

$$N_{B-L}^{\rm lep,f} \simeq \left[\frac{K_{2e}}{K_{2\tau_2^\perp}}\,\varepsilon_{2\tau_2^\perp}\kappa(K_{2\tau_2^\perp}) + \left(\varepsilon_{2e} - \frac{K_{2e}}{K_{2\tau_2^\perp}}\,\varepsilon_{2\tau_2^\perp}\right)\kappa(K_{2\tau_2^\perp}/2)\right] e^{-\frac{3\pi}{8}K_{1e}}$$
$$+ \left[\frac{K_{2\mu}}{K_{2\tau_2^\perp}}\,\varepsilon_{2\tau_2^\perp}\kappa(K_{2\tau_2^\perp}) + \left(\varepsilon_{2\mu} - \frac{K_{2\mu}}{K_{2\tau_2^\perp}}\,\varepsilon_{2\tau_2^\perp}\right)\kappa(K_{2\tau_2^\perp}/2)\right] e^{-\frac{3\pi}{8}K_{1\mu}}$$
$$+ \varepsilon_{2\tau}\,\kappa(K_{2\tau})\,e^{-\frac{3\pi}{8}K_{1\tau}}\,, \tag{36}$$

where $K_{2\tau_2^\perp} \equiv K_{2e} + K_{2\mu}$ and $\varepsilon_{2\tau_2^\perp} \equiv \varepsilon_{2e} + \varepsilon_{2\mu}$. The baryon-to-photon number ratio can then be simply calculated as $\eta_B \simeq 0.01\, N_{B-L}^{\rm lep,f}$. This is true assuming that any contribution from external sources can be neglected, a point that we will address in detail when we will discuss the strong thermal leptogenesis condition.

4.2. Flavoured CP asymmetries

It is now interesting to calculate the N_2 (flavoured) *CP* asymmetries within $SO(10)$-inspired models and in particular to see how these are linked to the low energy neutrino parameters. Defining them as

$$\varepsilon_{2\alpha} \equiv -\frac{\Gamma_{2\alpha} - \overline{\Gamma}_{2\alpha}}{\Gamma_2 + \overline{\Gamma}_2}\,, \tag{37}$$

these can be calculated from [44]

$$\varepsilon_{2\alpha} \simeq \bar{\varepsilon}(M_2)\left\{\mathcal{I}_{23}^{\alpha}\,\xi(M_3^2/M_2^2) + \mathcal{J}_{23}^{\alpha}\,\frac{2}{3(1-M_2^2/M_3^2)}\right\}, \tag{38}$$

where we introduced

$$\bar{\varepsilon}(M_2) \equiv \frac{3}{16\pi}\,\frac{M_2\, m_{\rm atm}}{v^2}\,, \qquad \xi(x) = \frac{2}{3}x\left[(1+x)\ln\left(\frac{1+x}{x}\right) - \frac{2-x}{1-x}\right], \tag{39}$$

$$\mathcal{I}_{23}^{\alpha} \equiv \frac{{\rm Im}\left[m_{D\alpha 2}^{\star} m_{D\alpha 3}(m_D^{\dagger} m_D)_{23}\right]}{M_2\, M_3\, \widetilde{m}_2\, m_{\rm atm}} \quad \text{and} \quad \mathcal{J}_{23}^{\alpha} \equiv \frac{{\rm Im}\left[m_{D\alpha 2}^{\star} m_{D\alpha 3}(m_D^{\dagger} m_D)_{32}\right]}{M_2\, M_3\, \widetilde{m}_2\, m_{\rm atm}}\,\frac{M_2}{M_3}, \tag{40}$$

with $\widetilde{m}_2 \equiv (m_D^{\dagger} m_D)_{22}/M_2$. Since in our case $M_3 \gg M_2$, we can use the approximation $\xi(M_3^2/M_2^2) \simeq 1$ and neglect the second term $\propto \mathcal{J}_{23}^{\alpha}$. Moreover, making use of the bi-unitary parameterisation (cf. Eq. (3)) and the approximation $V_L \simeq I$, one arrives to the following approximated expression for the flavoured *CP* asymmetries in $SO(10)$-inspired models,

$$\varepsilon_{2\alpha} \simeq \bar{\varepsilon}(M_2)\,\frac{m_{D\alpha}^2}{m_{D3}^2\,|U_{R32}|^2 + m_{D2}^2}\,\frac{|(m_\nu^{-1})_{\tau\tau}|^{-1}}{m_{\rm atm}}\,{\rm Im}[U_{R\alpha 2}^{\star}\,U_{R\alpha 3}\,U_{R32}^{\star}\,U_{R33}]\,. \tag{41}$$

Using the approximated expression Eq. (31) for U_R and the relations (4), one finds the following hierarchical pattern for the $\varepsilon_{2\alpha}$'s:

$$\varepsilon_{2\tau} : \varepsilon_{2\mu} : \varepsilon_{2e} = \alpha_3^2\, m_t^2 : \alpha_2^2\, m_c^2 : \alpha_1^2\, m_u^2\,\frac{\alpha_3 m_t}{a_2\, m_c}\,\frac{\alpha_1^2\, m_u^2}{\alpha_2^2\, m_c^2}\,. \tag{42}$$

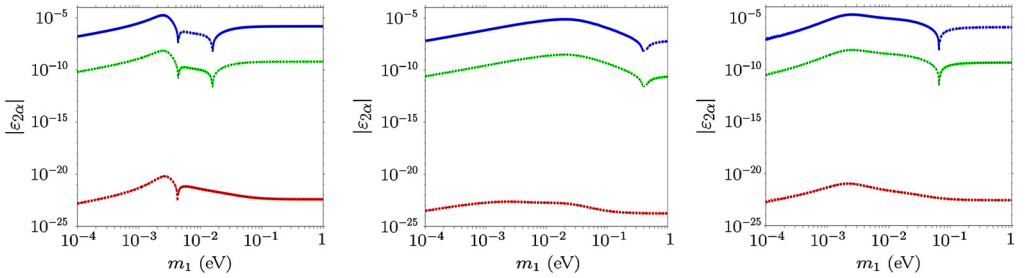

Fig. 3. Plots of the *CP* flavoured asymmetries corresponding respectively to the same three sets of parameters of Fig. 2. The solid coloured lines are the numerical curves (blue, green and red lines correspond respectively to tauon, muon and electron flavours). The dashed lines are the analytical expressions Eqs. (41). (For interpretation of the references to colour in this figure legend, the reader is referred to the web version of this article.)

As one can see, while $\varepsilon_{2\mu}$ is suppressed by about four orders of magnitude ($\sim m_c^2/m_t^2$) compared to $\varepsilon_{2\tau}$, the electronic *CP* asymmetry is suppressed even by about seven orders of magnitude compared to $\varepsilon_{2\mu}$. For this reason the electron contribution to the final asymmetry is always completely negligible.[11] This is well shown in Fig. 3 where, for the same four sets of parameters of Fig. 2, the flavoured (and total) *CP* asymmetries are plotted versus m_1, comparing the numerical result (solid lines) with the analytic expressions Eq. (41) (dashed lines). One can see how the analytic expressions again reproduce very well the numerical results. In particular one can recognise the hierarchical pattern Eq. (42).

5. Successful leptogenesis condition

In this section we finally impose the successful leptogenesis condition finding some first interesting constraints on the low energy parameters. In this respect we extend the results found in the hierarchical (LH) neutrino masses limit [18,19] to arbitrary values of m_1. The final asymmetry should be calculated using Eq. (36). However, as we have seen, in the approximation $V_L \simeq I$ the tauon *CP* asymmetry is by far the dominant one and the inclusion of the wash-out at the production cannot change the τ-dominance as a contribution to the final $B-L$ asymmetry. However, it should be stressed that this result holds using the $V_L \simeq I$ approximation, while relaxing this approximation, a muon-dominated solution also appears for $m_1 \gtrsim 10$ meV [19]. In any case the ST condition will select the tauon-dominated solution anyway and for this reason we can neglect the muon-dominated solution in our discussion. In this way the expression for the final asymmetry Eq. (36) greatly simplifies into

$$N_{B-L}^{\rm lep,f} \simeq \varepsilon_{2\tau}\, \kappa(K_{2\tau})\, e^{-\frac{3\pi}{8} K_{1\tau}}\,. \tag{43}$$

Using the explicit expressions Eqs. (31) and (34) for the U_R and Ω matrices respectively, we are now able to express the final $B-L$ asymmetry in $SO(10)$-inspired models in terms of the α_i and the low energy neutrino parameters.

[11] It is curious to notice that since the contribution to ε_{2e} from the interference with N_3 is so suppressed, actually it becomes comparable to the term coming from the interference with N_1 that we are neglecting in Eq. (38).

5.1. Final asymmetry in terms of the low energy neutrino parameters

Let us start from the derivation of an expression of $\varepsilon_{2\tau}$. First of all we can specialise Eq. (41) to the case $\alpha = \tau$, obtaining

$$\varepsilon_{2\tau} \simeq \frac{3}{16\pi}\,\frac{M_2}{v^2}\,\frac{m_{D3}^2}{m_{D3}^2\,|U_{R32}|^2 + m_{D2}^2}\,\frac{1}{|(m_\nu^{-1})_{\tau\tau}|}\,\mathrm{Im}[(U_{R32}^\star\,U_{R33})^2]\,. \tag{44}$$

Using then the expressions found for U_R and M_2, we arrive to

$$\varepsilon_{2\tau} \simeq \frac{3}{16\pi}\,\frac{\alpha_2^2\,m_c^2}{v^2}\,\frac{|m_{vee}|\,(|m_{\nu\tau\tau}^{-1}|^2 + |m_{\nu\mu\tau}^{-1}|^2)^{-1}}{m_1\,m_2\,m_3}\,\frac{|(m_\nu^{-1})_{\mu\tau}|^2}{|(m_\nu^{-1})_{\tau\tau}|^2}\,\sin\alpha_L\,, \tag{45}$$

where we have introduced the *effective SO*(10)*-inspired leptogenesis phase* α_L (in the approximation $V_L = I$)

$$\alpha_L \equiv 2\,\mathrm{Arg}[(m_\nu^{-1})_{\tau\tau}] - 2\,\mathrm{Arg}[(m_\nu^{-1})_{\mu\tau}] + \Phi_2 - \Phi_3\,, \tag{46}$$

and where from Eqs. (23) and (32) one has

$$\Phi_2 - \Phi_3 = \mathrm{Arg}\,[m_{vee}] - 2\,\mathrm{Arg}\left[(m_\nu^{-1})_{\tau\tau}\right] + \pi - 2\,(\rho+\sigma)\,, \tag{47}$$

so that we can write for the effective leptogenesis phase

$$\alpha_L = \mathrm{Arg}\,[m_{vee}] - 2\,\mathrm{Arg}[(m_\nu^{-1})_{\mu\tau}] + \pi - 2\,(\rho+\sigma)\,. \tag{48}$$

Let us now calculate the efficiency factor at the production $\kappa(K_{2\tau})$. First of all, from the expression Eq. (8), one can easily find, for $V_L \simeq I$, a general expression for the $K_{i\alpha}$'s,

$$K_{i\alpha} \simeq \frac{m_{D\alpha}^2}{m_\star\,M_i}\,|U_{R\alpha i}|^2\,. \tag{49}$$

From this one we can then obtain a specific expression for

$$K_{2\tau} \simeq \frac{m_{D3}^2}{m_\star\,M_2}\,|U_{R32}|^2 \simeq \frac{m_1\,m_2\,m_3}{m_\star}\,\frac{|(m_\nu^{-1})_{\mu\tau}|^2}{|m_{vee}|\,|(m_\nu^{-1})_{\tau\tau}|}\,, \tag{50}$$

where in the second approximation we made use of Eqs. (31) and (28).

From the general expression Eq. (49) we can also write an expression for $K_{1\tau}$ describing the exponential suppression of the lightest RH neutrino wash-out (cf. Eq. (43))

$$K_{1\tau} \simeq \frac{m_{D3}^2}{m_\star\,M_1}\,|U_{R31}|^2 \simeq \frac{|m_{ve\tau}|^2}{m_\star\,|m_{vee}|} = \frac{|m_1\,U_{e1}\,U_{\tau1} + m_2\,U_{e2}\,U_{\tau2} + m_3\,U_{e3}\,U_{\tau3}|^2}{m_\star\,|m_1\,U_{e1}^2 + m_2\,U_{e2}^2 + m_3\,U_{e3}^2|}\,. \tag{51}$$

From this one we can then obtain an explicit expression in terms of the mixing angles and low energy phases that will prove useful,

$$K_{1\tau} \simeq \frac{|c_{13}\,c_{12}\,s_{12}\,s_{23}\,(m_1\,e^{2\,i\,\rho} - m_2) + s_{13}\,c_{13}\,c_{23}\,(m_3\,e^{i\,(2\sigma-\delta)} - m_2\,s_{12}^2\,e^{i\,\delta} - m_1\,c_{12}^2\,e^{i\,(2\,\rho+\delta)})|^2}{m_\star\,|m_1\,c_{12}^2\,c_{13}^2\,e^{2\,i\,\rho} + m_2\,s_{12}^2\,c_{13}^2 + m_3\,s_{13}^2\,e^{2\,i\,(\sigma-\delta)}|}\,. \tag{52}$$

We can then finally put together all the results finding, from Eq. (43), an expression in terms of the low energy neutrino parameters that can be written as

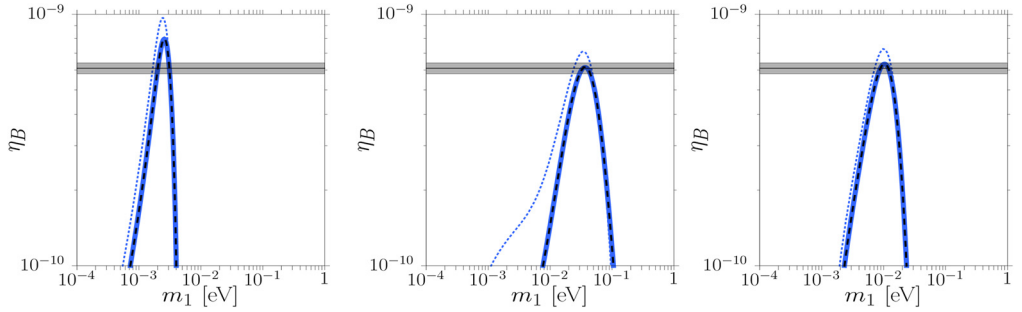

Fig. 4. Plots of the final η_B for the same three sets of parameters of Figs. 2 and 3. The numerical results (blue solid lines) are compared with the analytical results (black dashed lines) obtained using Eq. (53). The dotted lines are obtained switching on $V_L \neq I$. Using the same parameterisation for V_L as for U, in the three cases from left to right one has $\theta_{12}^L = (0.79°, 4.1°, 0.1°)$, $\theta_{13}^L = (0, 0.05°, 0.07°)$, $\theta_{23}^L = (2.3°, 2.3°, 2.3°)$, $\delta_L/\pi = (0.2, 0.63, 1.22)$, $\rho_L/\pi = (1.65, 0.85, 0.79)$ and $\sigma_L/\pi = (1.05, 1.1, 0.94)$. (For interpretation of the references to colour in this figure legend, the reader is referred to the web version of this article.)

$$N_{B-L}^{\rm lep,f} \simeq \frac{3}{16\pi}\,\frac{\alpha_2^2 m_c^2}{v^2}\,\frac{|m_{vee}|\,(|m_{\nu\tau\tau}^{-1}|^2 + |m_{\nu\mu\tau}^{-1}|^2)^{-1}}{m_1 m_2 m_3}\,\frac{|m_{\nu\tau\tau}^{-1}|^2}{|m_{\nu\mu\tau}^{-1}|^2}\,\sin\alpha_L$$
$$\times\,\kappa\left(\frac{m_1 m_2 m_3}{m_\star}\,\frac{|(m_\nu^{-1})_{\mu\tau}|^2}{|m_{vee}|\,|(m_\nu^{-1})_{\tau\tau}|}\right)$$
$$\times\, e^{-\frac{3\pi}{8}\,\frac{|m_{ve\tau}|^2}{m_\star |m_{vee}|}}\,. \tag{53}$$

It is interesting to notice that:

- The asymmetry does not depend on α_1 and on α_3 [18]. This is an important point since the only left non-observable parameter is α_2 on which however one can place a lower bound and, within $SO(10)$-inspired models cannot be in any case too large.
- The effective neutrinoless double beta decay mass $m_{ee} \equiv |m_{vee}|$ plays a direct role and it can be noticed that successful leptogenesis implies the existence of a lower bound.
- The successful leptogenesis condition links together all low energy neutrino parameters constraining them to lie on a hypersurface described by the only left theoretical parameter α_2.

In Fig. 4 we have plotted η_B vs. m_1 for the same three sets of parameters of Figs. 2 and 3 comparing the numerical results (blue solid lines) with the analytical results (black dashed lines) obtained from Eq. (53). As one can see the analytical results perfectly match the numerical ones.

We also made a more general comparison between the constraints derived from the analytical expression Eq. (53) and the numerical constraints (for $V_L = I$). In Fig. 5 we show, with orange points, the results of a scatter plot for $V_L = I$ imposing successful $SO(10)$-inspired leptogenesis for $\alpha_2 = 5$. The asymmetry is calculated from Eq. (43) where RH neutrino masses and mixing matrix U_R are calculated numerically. The mixing angles are uniformly random generated within the same ranges adopted in [18],

$$0 \leq \theta_{13} \leq 11.5°\,,\;\; 35° \leq \theta_{23} \leq 52°\,,\;\; 31.3° \leq \theta_{12} \leq 36.3°\,, \tag{54}$$

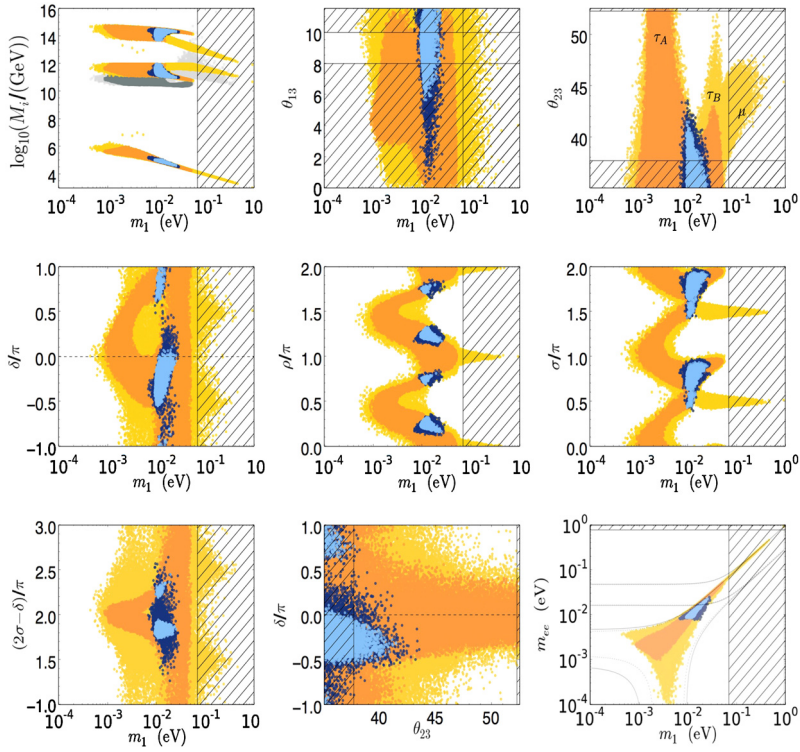

Fig. 5. Scatter plots in the low energy neutrino parameter space projected on different selected planes for NO and $\alpha_2 = 5$. The orange points respect the successful leptogenesis condition $\eta_B^{\rm lep} > \eta_B^{\rm CMB} > 5.9 \times 10^{-10}$ for $V_L = I$ where $\eta_B^{\rm lep}$ is calculated from Eq. (43) using a numerical determination of RH neutrino masses, mixing matrix and phases. The mixing angles vary within the ranges Eqs. (54). The blue points are those respecting the additional ST condition within the approximation $V_L = I$ (light blue) or for $I \leq V_L \leq V_{CKM}$ (dark blue). The dashed regions indicate either the values of m_1 excluded by the CMB upper bound (cf. Eq. (10)), or the values of m_{ee} excluded by $0\nu\beta\beta$ experiments, or the values of θ_{13} and θ_{23} excluded by current determination at 3σ (cf. Eq. (13)). In the bottom right panel the dashed (solid) black lines indicate the general (no leptogenesis) allowed bands, both for NO and IO, in the plane m_{ee} vs. m_1 for θ_{13} in the range in Eq. (54). (For interpretation of the references to colour in this figure legend, the reader is referred to the web version of this article.)

with the only exception of θ_{23} that is allowed to be slightly lower, as adopted in [17]. The results confirm those obtained in [18,19], simply here a much higher (about thousand times) amount of points has been obtained and the constraints are much sharper.

We have then produced corresponding scatter plots using directly the analytical expression for the final asymmetry Eq. (53). The results are shown in Fig. 6 and as one can see they perfectly reproduce the numerical results shown in Fig. 5 (orange points). We have also checked that one has a lower bound $\alpha_2 \gtrsim 3$ confirming the numerical result found in [18]. We can then conclude that Eq. (53) provides a very precise analytical way to calculate the final asymmetry in $SO(10)$-inspired models (we are excluding crossing level solutions from our analysis) in the approximation $V_L \simeq I$ and can be regarded as one of the main results of our investigation. Indeed it can reliably be applied in all models where $SO(10)$-inspired conditions hold in order impose the successful leptogenesis condition using directly predictions on low energy neutrino data (the only additional parameter that has to be calculated is α_2).

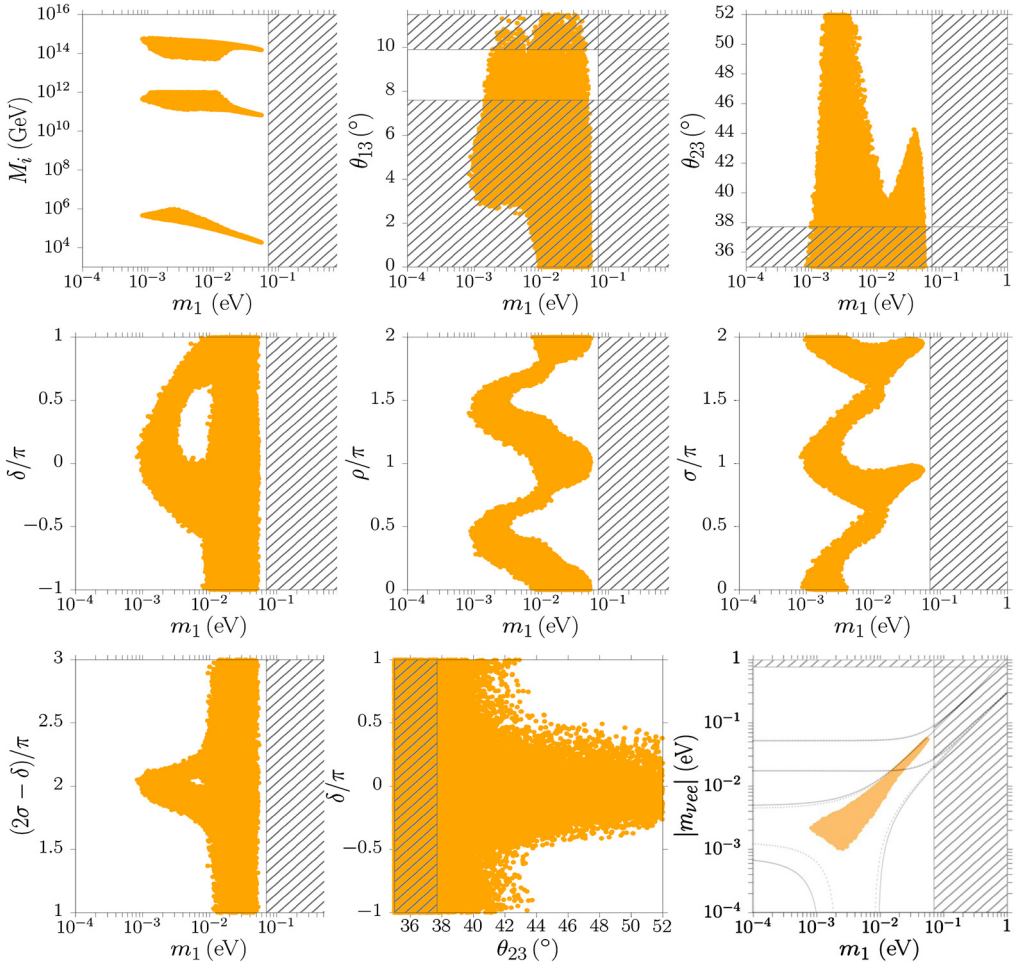

Fig. 6. Scatter plots in the low energy neutrino parameter space projected on different selected planes for NO and $\alpha_2 = 5$ respecting the successful leptogenesis condition $\eta_B^{\rm lep} > \eta_B^{\rm CMB} > 5.9 \times 10^{-10}$ and obtained from the analytical expression Eq. (53) for the final asymmetry. Same ranges and conventions as in Fig. 5 are adopted. These analytical results should be compared with the numerical results of Fig. 5 (orange points). (For interpretation of the references to colour in this figure legend, the reader is referred to the web version of this article.)

Having done this important cross check, we can now safely proceed further deriving analytical constraints on the low energy neutrino parameters imposing successful leptogenesis fully trusting our Eq. (53). Because of the intricate dependence of Eq. (53) on the low energy neutrino parameters, we need to understand the behaviour at low and high m_1 values, respectively for $m_1 \ll m_{\rm sol}$ and $m_1 \gg m_{\rm sol} \simeq 10\,{\rm meV}$ and then match the results for intermediate values $m_1 \simeq m_{\rm sol} \simeq 10\,{\rm meV}$.

5.2. *Lower bound on m_1*

Let us now calculate the final asymmetry in the limit $m_1 \to 0$ showing that this tends to vanish and, therefore, that successful $SO(10)$-inspired leptogenesis implies a lower bound on the

absolute neutrino mass scale [19]. It is convenient to start from $K_{1\tau}$. In the limit $m_1/m_{\rm sol} \to 0$ Eq. (51) simplifies into

$$K_{1\tau} \simeq \frac{1}{m_\star} \frac{|m_{\rm atm}\, s_{13}\, c_{13}\, c_{23}\, e^{i\,(2\sigma-\delta)} - m_{\rm sol}\, c_{13}\, s_{12}\, c_{12}\, s_{23}|^2}{|m_{\rm sol}\, s_{12}^2\, c_{13}^2 + m_{\rm atm}\, s_{13}^2\, e^{2i\,(\sigma-\delta)}|}\,. \tag{55}$$

From this result, we can see that the condition $K_{1\tau} \lesssim 1$ is verified for $2\sigma - \delta \simeq 2\pi\, n$ and

$$s_{13} \gtrsim \frac{m_{\rm sol}}{m_{\rm atm}}\, s_{12}\, c_{12}\, \tan\theta_{23} \gtrsim 0.06\,, \;\; \text{implying } \theta_{13} \gtrsim 3^\circ\,, \tag{56}$$

a lower bound that confirms the results of the scatter plots, first obtained in [18], shown in the top central panel of Figs. 5 and 6 in the plane $m_1 - \theta_{13}$.

We can now consider the low m_1 limit of $\varepsilon_{2\tau}$, obtaining from Eq. (45),

$$\varepsilon_{2\tau} \simeq \frac{3}{16\pi} \frac{\alpha_2^2\, m_c^2}{v^2} \frac{m_1}{m_{\rm sol}\, m_{\rm atm}} \frac{|m_{\rm sol}\, U_{e2}^2 + m_{\rm atm}\, U_{e3}^2|\, |U_{\mu 1}|^2}{|U_{\tau 1}|^2\, (|U_{\tau 1}|^4 + |U_{\mu 1}|^2\, |U_{\tau 1}|^2)} \sin\alpha_L \tag{57}$$

$$\simeq \frac{3}{16\pi} \frac{\alpha_2^2\, m_c^2}{v^2} \frac{m_1}{m_{\rm sol}\, m_{\rm atm}} \frac{|m_{\rm sol}\, s_{12}^2\, c_{13}^2 + m_{\rm atm}\, s_{13}^2\, e^{2\,i\,(\sigma-\delta)}|\, c_{23}^2}{s_{12}^4\, s_{23}^4} \sin\alpha_L\,, \tag{58}$$

where the asymptotic limit for the effective leptogenesis phase is given by $\alpha_L \simeq 2\,(\rho - \sigma)$.

Notice that we have retained the term $\propto s_{13}$ in m_{ee} since, as we have seen, it has to be non-vanishing. The expression is maximised for $\sigma - \delta \simeq n\,\pi$ with n integer and clearly for $\sin\alpha_L = 1$, finding

$$\varepsilon_{2\tau} \lesssim \frac{75}{16\pi} \frac{\alpha_2^2\, m_c^2}{v^2} \left(\frac{\alpha_2}{5}\right)^2 \frac{m_1}{m_{\rm atm}} \frac{c_{23}^2}{s_{12}^2\, s_{23}^4} \left(1 + \frac{m_{\rm atm}\, s_{13}^2}{m_{\rm sol}\, s_{12}^2}\right). \tag{59}$$

Finally the asymptotic limit for $K_{2\tau}$ for $m_1/m_{\rm sol} \ll 1$ is given by $K_{2\tau} \simeq c_{23}^2\, m_{\rm atm}/m_\star \simeq 25$ [18]. This shows that in the low m_1 limit the wash-out at the production is strong and in this case one can use a simple approximation for the efficiency factor [7], $\kappa(K_{2\tau}) \simeq 0.5/K_{2\tau}^{1.2} \simeq 0.01$. Combining together the results found for the three terms, one finds that in the low m_1 limit the baryon-to-photon number ratio is maximised by

$$\eta_B^{\rm lep} < \eta_B^{\rm max} \simeq 10^{-4} \frac{75}{16\pi} \frac{\alpha_2^2\, m_c^2}{v^2} \left(\frac{\alpha_2}{5}\right)^2 \frac{m_1}{m_{\rm atm}} \frac{c_{23}^2}{s_{12}^2\, s_{23}^4} \left(1 + \frac{m_{\rm atm}\, s_{13}^2}{m_{\rm sol}\, s_{12}^2}\right) \tag{60}$$

$$\equiv m_1 \left(\frac{\alpha_2}{5}\right)^2 f(\theta_{12}, \theta_{13}, \theta_{23})\,. \tag{61}$$

Imposing finally the successful leptogenesis condition implying $\eta_B^{\rm max} \gtrsim \eta_B^{\rm CMB}$, one obtains the lower bound

$$m_1 \gtrsim 6 \times 10^{-10} \left(\frac{5}{\alpha_2}\right)^2 [f(\theta_{12}, \theta_{13}, \theta_{23})]^{-1} \gtrsim 0.08\ {\rm meV} \left(\frac{5}{\alpha_2}\right)^2, \tag{62}$$

where the last inequality has been obtained for the values of the mixing angles within the ranges Eq. (54) that minimise $[f(\theta_{12}, \theta_{13}, \theta_{23})]^{-1}$. The result is in very good agreement with the results of the scatter plots shown in Fig. 5 (orange points) and Fig. 6 and confirms, in more detail, the value obtained in [18].

Finally it should be noticed that the three conditions for maximal asymmetry on the three low energy phases, $2\sigma - \delta \simeq m\,\pi$, $\sigma - \delta \simeq n\,\pi$ and $\sin[2\,(\rho - \sigma)] \simeq 1$, with n, m integers, imply

that in the low m_1 limit one has $\sigma = (2n - m)\pi$ and $\delta = 2\pi n$, results that are confirmed by the results, at low m_1, of the scatter plot shown in the two panels in Fig. 5 (and Fig. 6 as well) for σ and δ vs. m_1 (orange points). One also finds $\rho = \pi/4 + q\pi$, with q integer. It can be seen however that at small m_1 the value of ρ is actually $\rho \simeq 0.35\pi + q\pi$. The reason for this shift is understood from the more complete expression Eq. (52) for $K_{1\tau}$. For $\rho = \pi/2$ the term $m_1 e^{2i\pi\rho} = -m_1$ adds to the term $-m_2$ in a way that $K_{1\tau} \lesssim 1$ for slightly lower values of s_{23}. In this way, because of the strong dependence $\varepsilon_{2\tau} \propto s_{23}^{-4}$, a shift of ρ towards $\pi/2$ maximises the asymmetry even though the phase α_L is not maximal. We will be back soon on the fact that value of θ_{23} cannot be too large.

5.3. Upper bound on m_1

Together with a lower bound on m_1, there is also an upper bound on m_1. We can work in the quasi-degenerate neutrino limit $m_1 \simeq m_2 \simeq m_3$ and then check whether the upper bound does indeed fall in the quasi-degenerate regime.

Let us first calculate separately the quasi-degenerate limit of $K_{1\tau}$, $K_{2\tau}$ and $\varepsilon_{2\tau}$, the three relevant quantities determining the final asymmetry. For $K_{1\tau}$ from Eq. (52) one can immediately see that if $\rho = n\pi$, with n integer, then

$$K_{1\tau} \simeq s_{13}\, c_{23}^2\, \frac{m_1}{m_\star} \left| e^{i(2\sigma-\delta)} - s_{12}^2 - c_{12}^2 e^{i\delta} \right|^2 \lesssim 0.015\, \frac{m_1}{m_\star} \left| e^{i(2\sigma-\delta)} - s_{12}^2 - c_{12}^2\, e^{i\delta} \right|^2 . \quad (63)$$

This expression shows that for $m_1 \lesssim 0.1$ eV one has $K_{1\tau} \lesssim 4$, where the maximum is saturated for $\sigma = 2\pi\, m$ and $\delta = \pi/2 + k\pi$, so in any case it cannot be too large and it can be always made vanishing.

Let us now calculate the asymptotic limit of $\varepsilon_{2\tau}$ for $\rho \simeq n\pi$. We can neglect all sub-dominant terms $\propto s_{13}^2$ containing δ in a way that the dependence on δ cancels out. First of all notice that $m_{ee} \equiv |m_{vee}| \to m_1$ an asymptotic limit that is clearly visible in the panels of Figs. 5 and 6. At the same time one has,

$$\left| (m_\nu^{-1})_{\tau\tau} \right|^2 \to \frac{1}{m_1^2} \left| s_{23}^2 + c_{23}^2\, e^{-2\,i\,\sigma} \right|^2 , \quad (64)$$

$$\left| (m_\nu^{-1})_{\mu\tau} \right|^2 \to \frac{s_{23}^2\, c_{23}^2}{m_1^2} \left| e^{-2\,i\,\sigma} - 1 \right|^2 . \quad (65)$$

In this way putting all terms together one finds from Eq. (45) the following asymptotic limit for $\varepsilon_{2\tau}$

$$\varepsilon_{2\tau} \to \frac{3}{16\pi}\, \frac{\alpha_2^2\, m_c^2}{v^2}\, \frac{s_{23}^2\, c_{23}^2\, |e^{-2i\sigma} - 1|^2 / |s_{23}^2 + c_{23}^2\, e^{-2i\sigma}|^2}{(|s_{23}^2 + c_{23}^2\, e^{-2i\sigma}|^2 + s_{23}^2\, c_{23}^2\, |e^{-2i\sigma} - 1|^2)}\, \sin\alpha_L , \quad (66)$$

where the asymptotic limit of α_L is given by $\alpha_L \to -4\sigma$.

Finally we can calculate the asymptotic limit of $K_{2\tau}$ from Eq. (50), finding

$$K_{2\tau} \to \frac{m_1}{m_\star}\, \frac{s_{23}^2\, c_{23}^2\, |e^{-2i\sigma} - 1|^2}{|s_{23}^2 + c_{23}^2\, e^{-2\,i\,\sigma}|} . \quad (67)$$

Putting all together in Eq. (43) for $N_{B-L}^{\rm lep,f}$, using the approximation $\kappa(K_{2\tau}) \simeq (1 + 2\, K_{2\tau}^{1.2})^{-1}$ and considering that $\eta_B \simeq 0.01\, N_{B-L}^{\rm p,f}$ one finds as asymptotic limit for η_B,

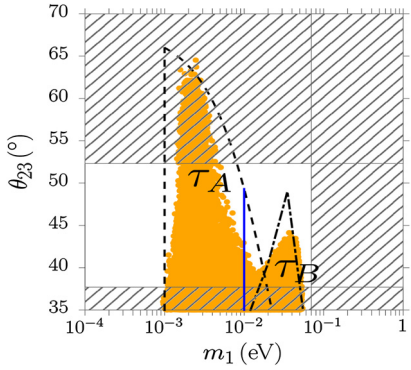

Fig. 7. Scatter plot in the plane $m_1 - \theta_{23}$ obtained imposing successful $SO(10)$-inspired leptogenesis with the asymmetry calculated from the analytic Eq. (53) as in the previous figure but with enlarged θ_{23} range. The dashed lines indicate the lower bound on m_1 Eq. (62) and the upper bound on θ_{23} at low m_1 Eq. (71). The dot-dashed lines indicate the upper bound on m_1 Eq. (70) and the upper bound on θ_{23} at high m_1. As one can see, the two regions at low and high values of m_1, the type A and type B solutions respectively, overlap around $m_1 \sim 10$ meV. The solid line is the lower bound from the ST condition Eq. (81) for $N^{\rm p,i}_{B-L} = 10^{-3}$.

$$\eta_B \to \simeq \frac{0.03}{16\,\pi}\,\frac{\alpha_2^2\, m_c^2}{v^2}\,\frac{s_{23}^2\, c_{23}^2\, |e^{-2i\sigma}-1|^2/|s_{23}^2 + c_{23}^2\, e^{-2i\sigma}|^2}{(|s_{23}^2 + c_{23}^2\, e^{-2i\sigma}|^2 + s_{23}^2\, c_{23}^2\, |e^{-2i\sigma}-1|^2)}\,\frac{\sin\alpha_L}{1 + 2\, K_{2\tau}^{1.2}}\, e^{-\frac{3\pi}{8}\, K_{1\tau}}\,, \quad (68)$$

where, remember, we assumed $\rho = n\,\pi$.

Here we can notice that the asymptotic limit depends mainly on the value of σ, since in any case $\rho \simeq n\,\pi$ in order to have $K_{1\tau} \lesssim 1$ and here the residual dependence on δ can be neglected. Guessing that the value of σ that minimise $K_{2\tau}$ is such that $2\sigma \ll 1$ and using simply $\sin\alpha_L \lesssim 1$, one has that η_B, is maximised by

$$\eta_B \lesssim \frac{0.03}{16\,\pi}\,\frac{\alpha_2^2\, m_c^2}{v^2}\,\frac{x}{1 + 2\left(\frac{m_1}{m_\star}\right)^{1.2}\, x^{1.2}} \lesssim \frac{0.01}{192\,\pi}\,\frac{\alpha_2^2\, m_c^2}{v^2}\,\frac{m_\star}{m_1}\,, \quad (69)$$

where we defined $x \equiv s_{23}^2\, c_{23}^2\, |e^{-2i\sigma} - 1|^2$ and maximised on it finding $x = 2.5^{1.2}\,(m_\star/m_1)$, that indeed implies $\sigma \ll 1$ as guessed. Imposing successful leptogenesis one then straightforwardly finds the upper bound

$$m_1 \lesssim m_\star \left[\frac{2.5^{1.2} \times 10^8}{6 \times 32\,\pi}\,\frac{\alpha_2^2\, m_c^2}{v^2}\right] \lesssim 52\ \text{meV}\,, \quad (70)$$

very well reproducing the result from the scatter plots (Figs. 5, 6 and 7) even though it does not fall in a full quasi-degenerate regime. This upper bound is shown in Fig. 7 (dot-dashed line). In conclusion the upper bound on m_1 is mainly due to an interplay between minimising simultaneously both $K_{1\tau}$ and $K_{2\tau}$ while maximising the CP asymmetry. In the top-left panel of Fig. 8 a scatter plot of $K_{2\tau}$ vs. m_1 (orange points) confirms how for $m_1 \gtrsim 10$ meV the value of $K_{2\tau}$ becomes smaller and smaller for growing m_1 in order to minimise the wash-out at the production that suppresses the asymmetry $\propto m_\star/m_1$. The upper bound on m_1 is saturated for an analytical minimum value of $K_{2\tau} \simeq 2.5$ well in agreement with the numerical result.

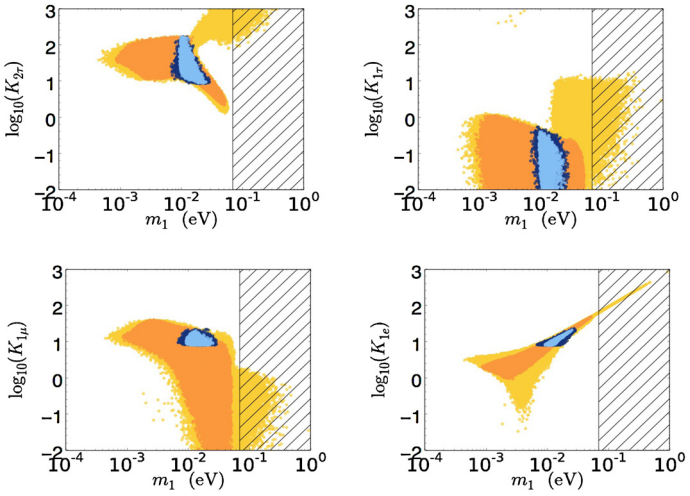

Fig. 8. Scatter plots for the four flavoured decay parameters $K_{2\tau}$, $K_{1\tau}$, K_{1e}, $K_{1\mu}$ vs. m_1. The colour code is the same as in Fig. 5. (For interpretation of the references to colour in this figure legend, the reader is referred to the web version of this article.)

5.4. *Type A solution ($m_1 \lesssim m_{\rm sol}$)*

We now describe what happens for values of m_1 between the lower and the upper bound. From this point of view, as we will see, the value of $m_{\rm sol} \simeq 10$ meV represents a kind of border between two different solutions, the τ_A and the τ_B solutions, though the border is not sharp and the two solutions overlap somehow around $m_1 \simeq 10$ meV. This distinction will be useful when we will discuss the ST solution in the next section. Let us start from values $m_1 \lesssim m_{\rm sol}$.

5.4.1. *Upper bound on θ_{23}*

An important feature of $SO(10)$-inspired leptogenesis is that, for NO as we are considering, it places an upper bound on θ_{23}. In the case of low values of $m_1 \lesssim m_{\rm sol}$, from Eq. (55), imposing $K_{1\tau} \lesssim 1$ and taking into account the dominant term $\propto m_1 e^{2i\rho}$ in $K_{1\tau}$, and approximating $\rho \simeq \pi/2$, one finds the upper bound

$$\theta_{23} \lesssim \arctan\left[\frac{m_{\rm atm} - m_{\rm sol}\, s_{12}^2}{m_{\rm sol} + m_1}\,\frac{s_{13}}{c_{12}\, s_{12}}\right] \lesssim 65^\circ\,, \tag{71}$$

where the maximum value on the right-hand side is obtained clearly in the limit $m_1/m_{\rm sol} \to 0$. In Fig. 7 we show the results of a specific scatter plot obtained starting from the analytic Eq. (53), holding for $V_L \simeq I$, in the plane $m_1 - \theta_{23}$, as for Fig. 5 but this time with θ_{23} in the range $35^\circ \lesssim \theta_{23} \lesssim 70^\circ$. It can be seen how the analytical upper bound Eq. (71) well reproduces the numerical result.

5.4.2. *Sign of the asymmetry and low energy phases*

Here we want to show how the sign of the asymmetry influences the values of the phases. Looking at the $K_{i\alpha}$ one could indeed think that constraints on ρ and σ should exhibit a $\pi/2$-periodicity while constraints on δ a π-periodicity. This is because the $K_{i\alpha}$ are defined in absolute values and an overall change of sign of the argument leaves them unchanged. However,

it can be seen from the Figs. 5 and 6 that actually σ and ρ constraints have a π-periodicity and constraints on δ have a 2π-periodicity. This is an effect of the sign of the asymmetry that, looking at Eq. (53), is clearly given by

$$\text{sign}(\eta_B) = \text{sign}(\alpha_L)\,. \tag{72}$$

For the τ_A solution, for $m_1 \ll m_{\rm sol}$, one has $\alpha_L \simeq 2\,(\rho - \sigma)$ and, therefore, one has that $\rho - \sigma \simeq \pi/4$ would maximise the asymmetry. We have already discussed how in the limit of lowest m_1 the value of $\rho \simeq 0.35\,\pi$ while indeed the value of $\sigma \simeq 0.1\,\pi$. This is because values $\rho = \pi/2$ would maximise the amplitude of the *CP* asymmetry and at the same time minimise $K_{1\tau}$. Values $\rho \simeq 0.35\,\pi$ are, therefore, a compromise that maximise the total final asymmetry. At the same time the value $2\sigma - \delta \simeq 0$ in order to minimise $K_{1\tau}$, while $\sigma - \delta \simeq 0$ in order to maximise m_{ee}.

When $m_1/m_{\rm sol}$ increases, the values of the phases can be understood from Eq. (52) for $K_{1\tau}$. The first term in the numerator $\propto m_1\, e^{2\,i\,\rho}$ becomes non-negligible. Since ρ is slightly different from $\pi/2$, this term has some non-vanishing imaginary part that has also to be cancelled in order not to have $K_{1\tau} \gg 1$. Since, as we have seen, at low m_1 necessarily $s_{13} \neq 0$, this is cancelled by the term $\propto m_3\, e^{i\,(2\sigma - \delta)}$ with $2\sigma - \delta < 0$. For increasing values of m_1, the value of ρ has necessarily to tend to $\rho = n\,\pi$ in order to have $m_1 e^{2\,i\,\rho} - m_2 \simeq 0$. In this case there are two possibilities: either $\rho > \pi/2$ and in this case $2\sigma - \delta > 0$ or $\rho < \pi/2$ and in this case $2\sigma - \delta < 0$. The latter is clearly the dominant case, since, as we said, at lowest values of m_1 one has necessarily $\rho \simeq 0.35\pi < \pi/2$. For this case it is possible at the same time to have maximal phase and small value of $K_{1\tau}$. It is important to realise that the dominance of this case is driven by the *positive sign of the asymmetry*.

In order to make these visible from the scatter plots in a clear way, we have produced new scatter plots constraining the reactor mixing angle in the current 3σ experimental range (cf. Eq. (13)). The results are shown in Fig. 9. In the first (top-left) panel we show the ρ vs. m_1 scatter plot. One can first of all see that because of the much more restricted θ_{13} range, many points disappeared compared to the corresponding plot in Fig. 5 and the behaviour is much cleaner. At the lower bound $m_1 \simeq 1$ meV one can see how indeed $\rho \simeq 0.35\,\pi$. For increasing values of m_1 there are two branches for ρ: in a first 'high' branch the value of ρ increases to π and in a second 'low' branch it decreases to 0, where the two branches actually merge because of the π periodicity. It is clearly noticeable how the low branch dominates, since it corresponds to values of ρ that produce the correct sign of the asymmetry and to maximal leptogenesis phase (α_L) values already at minimum m_1-values, while the high-ρ branch is suppressed since it corresponds to non-maximal α_L values.

In the second (top-right) panel we show the $2\sigma - \delta$ scatter plot. This clearly shows how the 'low-ρ' branch corresponds to (dominant) $2\sigma - \delta$ values below $2\,n\pi$, while the 'high-ρ' branch corresponds to (sub-dominant) $2\sigma - \delta$ values greater than $2\,n\pi$.

The next step is to understand what are the corresponding values of σ. In the third panel of Fig. 9 we show the σ vs. m_1 scatter plot. As it could be expected by the fact that $\alpha_L \to 2(\rho - \sigma)$ for $m_1 \ll m_{\rm sol}$, the (sub-dominant) high ρ values branch corresponds to high sub-dominant σ values branch ($\sigma \gtrsim n\,\pi$) while the dominant low ρ values branch corresponds to a low (dominant) σ values branch.

Finally, combining these results on σ with the results shown on $2\sigma - \delta$, we can deduce the behaviour of δ. For the dominant low-ρ values branch, corresponding to a low-σ values branch and values of $2\sigma - \delta \lesssim 2\,n\,\pi$ one concludes that δ shifts toward negative values. Vice-versa the sub-dominant high ρ values branch, corresponding to $2\sigma - \delta > 2n\,\pi$ values and high $\sigma > m\,\pi$ values, one has positive δ values. The results are shown in the last (bottom-right) panel of Fig. 9.

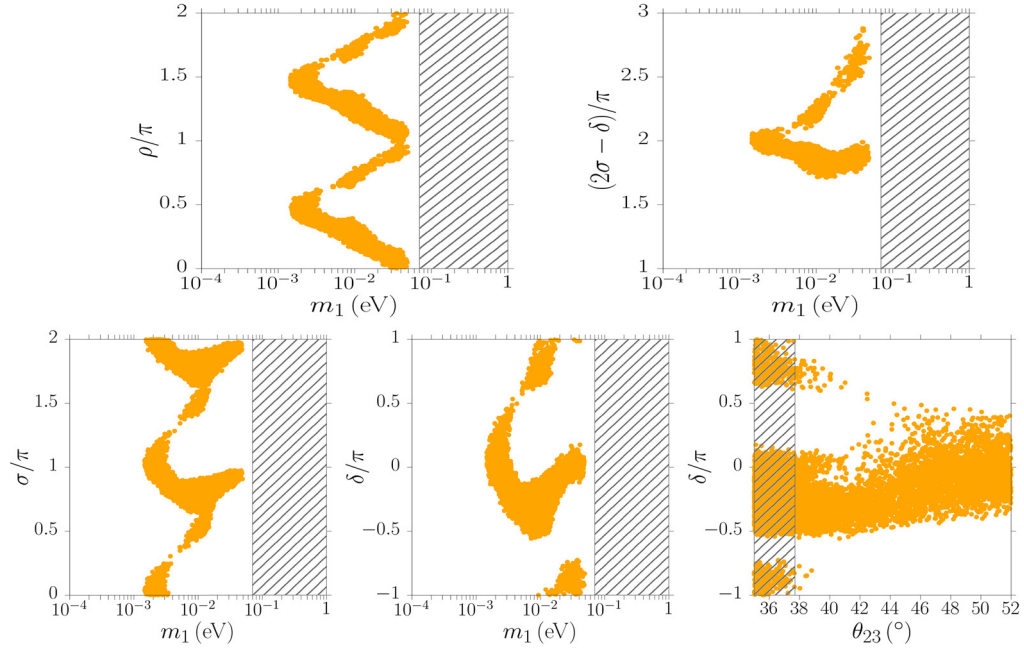

Fig. 9. Scatter plots of points satisfying successful leptogenesis generated using the analytical expression Eq. (53) for the final asymmetry in different planes. The mixing angle θ_{13} values are uniformly randomly generated within the 3σ allowed experimental range in Eq. (13). Panels should be compared with the corresponding ones in Fig. 6, in particular the last one for δ vs. θ_{23}.

One can see the clear dominance of values of δ in the fourth quadrant. This conclusion is strengthened even more by a scatter plot of δ vs. θ_{23} showing that actually positive values of δ are even more constrained if one imposes the current 3σ lower bound $\theta_{23} \gtrsim 38°$. This result should be mainly regarded as a proof that within $SO(10)$-inspired leptogenesis the sign of the asymmetry yields asymmetric constraints between positive and negative $\sin\delta$ values. However, it would be certainly interesting to see how these constraints relax going beyond the $V_L = I$ approximation since this could also provide quite an effective way to test $SO(10)$-inspired leptogenesis with future experimental results.

5.5. *Type B solution ($m_1 \gtrsim m_{\rm sol}$)*

Because of the upper bound $m_1 \lesssim m_{\rm atm}$, we can approximate $m_1 \simeq m_2$ and $m_3 \simeq m_{\rm atm}$. In this case the general expression for $K_{1\tau}$ Eq. (52) can be written as,

$$K_{1\tau} \simeq \frac{|c_{13}\, c_{12}\, s_{12}\, s_{23}\, m_1\, (e^{2\,i\,\rho}-1) + s_{13}\, c_{13}\, c_{23}\, e^{-i\,\delta}\, [m_{\rm atm}\, e^{i\,2\,(\sigma-\delta)} - m_1\, (s_{12}^2 + c_{12}^2\, e^{2\,i\,\rho})|]^2}{m_\star\, |m_1\, c_{13}^2 (c_{12}^2\, e^{2\,i\,\rho} + s_{12}^2) + m_{\rm atm}\, s_{13}^2\, e^{2\,i\,(\sigma-\delta)}|}\,. \tag{73}$$

There are two possibilities to minimise $K_{1\tau}$. In the case $s_{13} \to 0$ one can simply have $\rho = n\,\pi$ and this immediately produces $K_{1\tau} = 0$, showing that it is quite easy to find a way for the tauon asymmetry to escape the lightest RH neutrino wash-out. On the other hand for the measured values $s_{13} \simeq 0.15$ a non-vanishing value of the first term in the numerator is necessary in order

to cancel the second term. The exact value of ρ depends on the value of m_1. The value of δ is in this case able to cancel the imaginary part of $e^{2i\rho}$ but at the same time has to be such to keep $\sigma - \delta \simeq n\pi$ in order to maximise the value of m_{ee}. Moreover since $\alpha_L \simeq -4\sigma$ has to be negative, this also leads to negative values of δ and favours positive values of ρ. This is confirmed by the first panel of Fig. 9 showing a scatter plot of ρ vs. m_1 for θ_{13} in the 3σ range Eq. (13). It can be seen how this time, compared to the analogous plot of Fig. 5 where $0 \leq \theta_{13} \leq 11.54°$, one has $\rho = n\pi$ only when m_1 saturates its upper bound.

We can maximise $K_{1\tau}$ taking in both cases $\rho = n\pi$ even for $m_1 \simeq m_{\rm sol} \ll m_{\rm atm}$ and taking $\sigma - \delta = m\pi$ in order to maximise m_{ee}, and in this case one finds

$$K_{1\tau} \lesssim \frac{s_{13}^2\, c_{23}^2\, (m_{\rm atm} - m_1)^2}{m_\star\, (m_{\rm atm} + s_{13}^2\, m_{\rm atm})} \simeq 2\,, \tag{74}$$

showing that indeed the lightest RH neutrino wash-out can be avoided in any case.

Let us now consider the *CP* asymmetry $\varepsilon_{2\tau}$ and the wash-out at the production described by $K_{2\tau}$. In the expressions one can still approximate $m_{ee} \simeq m_1$, as for the quasi-degenerate case. However, this time one has

$$|(m_\nu^{-1})_{\tau\tau}| \simeq \frac{1}{m_1}\left|s_{23}^2 + \frac{m_1}{m_3}\, c_{23}^2\right| \quad \text{and} \quad |(m_\nu^{-1})_{\mu\tau}| \simeq \frac{s_{23}\, c_{23}}{m_1}\left|1 - \frac{m_1}{m_3}\right|, \tag{75}$$

where we have approximated $\sigma \simeq n\pi$. These two expressions produce a dependence $\eta_B \propto s_{23}^{-4}$ that strongly suppresses the asymmetry for increasing s_{23} and produces a tight upper bound on θ_{23}. On the other hand, however, now one also has $\eta_B \propto m_1/m_3$ and this makes in a way that the upper bound gets relaxed at higher m_1 reaching a maximum toward $m_1 \simeq 0.035$ meV. This is because for higher m_1 the term $|(m_\nu^{-1})_{\mu\tau}| \propto 1 - m_1/m_3$ suppresses the asymmetry.

Finally one also has

$$K_{2\tau} \simeq \frac{m_3}{m_\star}\, \frac{s_{23}^2\, c_{23}^2\, (1 - m_1/m_3)^2}{(s_{23}^2 + c_{23}^2\, m_1/m_3)}\,. \tag{76}$$

Combining together all results, one finds an implicit form for the upper bound of s_{23} vs. m_1. In Fig. 7 we have plotted with the dot-dashed line the result. As one can see it somehow overestimates the allowed region. This is a consequence of the crude approximations used for the phases. In any case these results well explain the existence of an upper bound on θ_{23} also for values $m_1 \gtrsim m_{\rm sol}$ and how this gets relaxed for increasing values of m_1 upto a peak value that is reached for $m_1 \simeq 35$ meV. For values $m_1 \gtrsim 35$ meV the upper bound on θ_23 vs. m_1 becomes more stringent and $\theta_{23}^{\rm max} \to 0$ when $m_1 \to m_1^{\rm max}$, where $m_1^{\rm max} \simeq 52$ meV is the upper bound Eq. (70) found in the quasi-degenerate limit. It should be noticed how the regions for the τ_A and for the τ_B solutions overlap to some extent for $m_1 \simeq 10$ meV. This is not contradictory since they are realised for different values of the phases, in particular in the case of the τ_A solution the phase $\rho \simeq \pi/2$ for $m_1 \to 0$, while for the τ_B solution one has $\rho \simeq \pi$ for $m_1 \simeq m_1^{\rm max}$. Around $m_1 \simeq 10$ meV the two solutions meet but, as we will discuss in the next section, the τ_B solution is incompatible with the ST leptogenesis condition.

6. Strong thermal leptogenesis condition

In this section we finally over-impose the ST condition in addition to the successful leptogenesis and $SO(10)$-inspired conditions, deriving all the features of the ST-$SO(10)$-inspired

solution [17]. All $SO(10)$-inspired solutions, for $V_L = I$, are already tauon-type solutions satisfying $K_{1\tau} \lesssim 1$. Therefore, we need to impose, in addition, the conditions Eqs. (9).

For pre-existing initial asymmetries $N^{\rm p,i}_{\Delta_\alpha}$ in the different flavours $\alpha = e, \mu, \tau$, one has to require [22]

$$K_{2\tau}\,, K_{1e}\,, K_{1\mu} \gtrsim \frac{8}{3\pi}\left[\ln\left(\frac{0.1}{\eta_B^{\rm CMB}}\right) + \ln\left|N^{\rm p,i}_{\Delta_\alpha}\right|\right] \simeq 8 + 0.85\,\ln\left|\frac{N^{\rm p,i}_{\Delta_\alpha}}{1.5\times 10^{-4}}\right|, \tag{77}$$

in order for these components to give a negligible contribution to the final asymmetry. Because of geometric factors in general a total pre-existing asymmetry $N^{\rm p,i}_{B-L}$ corresponds to values of the electron and muonic pre-existing asymmetries at the lightest RH neutrino wash-out of about $N^{\rm p,i}_{\Delta_\alpha} \simeq N^{\rm p,i}_{B-L}/6$ [22].

6.1. The τ_B solution cannot realise ST leptogenesis

First of all it is easy to show that the τ_B solutions, characterised by $m_1 \gtrsim 10$ meV and $\rho \simeq n\,\pi$ cannot satisfy the ST condition.

If one goes back to the expression (76) for $K_{2\tau}$ in the τ_B case, one can immediately check that for $m_1 \simeq m_{\rm sol}$ one has $K_{2\tau} \simeq 13$, that would be still sufficient to wash-out a pre-existing asymmetry as large as $\sim 10^{-2}$. The wash-out of a pre-existing electronic asymmetry is also not a problem. Indeed, starting from the expression Eq. (49) for the $K_{i\alpha}$ and using $M_1 = m^2_{D1}/m_{ee}$ (cf. Eq. (25)) and that $U_{R11} \simeq 1$, one immediately obtains, in general and therefore also for τ_B solutions, that $K_{1e} \simeq m_{ee}/m_\star \simeq m_1/m_\star$. This is sufficient to wash-out electronic pre-existing asymmetries as large as 10^{-3} for $m_1 \gtrsim 10$ meV and even larger if m_1 increases (as we will see soon this is indeed the origin of the lower bound on m_1). The real intrinsic problem for τ_B solutions is the wash-out of a pre-existing muon component, since one can easily see that

$$K_{1\mu}\big|_{\tau_B} \simeq \frac{m^2_{\rm atm}}{m_\star}\,\frac{s^2_{13}\,s^2_{23}}{|m_1 + s^2_{13}\,m_{\rm atm}|} \lesssim 4\,, \tag{78}$$

confirming in a general analytical way the numerical examples shown in [18,19,17]. Therefore, we conclude that τ_B-type solutions cannot realise ST leptogenesis because they cannot wash-out a large pre-existing muon asymmetry. We can then now focus on τ_A solutions in the following discussion.

6.2. Lower bounds on m_{ee} and on m_1

As we have just seen, one finds easily from the general expression Eq. (8) $K_{1e} = m_{ee}/m_\star$, interestingly showing how in $SO(10)$-inspired models a not too low neutrino-less double beta decay effective neutrino mass is required for the wash-out of the pre-existing electronic asymmetry. Indeed, from Eq. (77) we can immediately place the lower bound

$$m_{ee} \gtrsim 8\ {\rm meV}\left(1 + 0.095\,\ln\left|\frac{N^{\rm p,i}_{\Delta_e}}{1.5\times 10^{-4}}\right|\right), \tag{79}$$

that is quite interesting since it predicts that, despite neutrino masses are NO, next generation $0\nu\beta\beta$ experiments should find a signal. This lower bound translates into a lower bound on m_1. From the explicit general expression for m_{ee},

$$\begin{aligned} m_{ee} &= |m_1\, U_{e1}^2 + m_2\, U_{e2}^2 + m_3\, U_{e3}^2| \\ &= |m_1\, c_{12}^2\, c_{13}^2\, e^{2\,i\,\rho} + m_2\, s_{12}^2\, c_{13}^2 + m_3\, s_{13}^2\, e^{2\,i\,(\sigma-\delta)}| \\ &\simeq m_1\, |c_{12}^2\, e^{2\,i\,\rho} + s_{12}^2|\,, \end{aligned} \tag{80}$$

where we approximated $m_1 \simeq m_2$ and neglected the term $\propto m_3\, s_{13}^2$. Considering that for the τ_A type solutions one has $2\rho \simeq \pm\pi/2$, one arrives to $m_{ee}/m_1 \simeq \sqrt{c_{12}^4 + s_{12}^4} \simeq 0.75$, in very good agreement with the numerical results. From this result combined with the lower bound Eq. (79), one then obtains the lower bound

$$m_1 \gtrsim 10\ \text{meV} \left(1 + 0.095\, \ln \left| \frac{N_{\Delta_e}^{\text{p,i}}}{1.5 \times 10^{-4}} \right| \right). \tag{81}$$

This result is a specific example of what happens more generally, beyond $SO(10)$-inspired models, for NO: the wash-out of the electronic pre-existing asymmetry implies a lower bound on m_1 [22]. In the case of $SO(10)$-inspired models this lower bound is particularly stringent and implies $\sum_i m_i \gtrsim 75\,\text{meV}$, a prediction that will be tested by future cosmological observations.

6.3. Atmospheric mixing angle in the first octant and upper bound on m_1 and m_{ee}

Plugging the lower bound on m_1 Eq. (81) in Eq. (71) giving the upper bound on θ_{23}, one finds, for $N_{\Delta_e}^{\text{p,i}} = 10^{-3}$, the upper bound $\theta_{23} \lesssim 40^\circ$, quite in well agreement with the scatter plots in Fig. 5 (light blue points).

At the same time an upper bound on m_1 is found simply by the value of m_1 corresponding to the minimum value of θ_{23} in Eq. (81). For $\theta_{23} = 35^\circ$, as in the scatter plots in Fig. 5, one finds $m_1 \lesssim 20$ meV. From this upper bound one can then straightforwardly write $m_{ee} \lesssim 0.8\, m_1 \lesssim 16$ meV, in fair agreement with the result from the scatter plots shown in Fig. 5 that give $m_1 \lesssim 23$ meV. This upper bound gets relaxed to $m_1 \lesssim 30$ meV going beyond the approximation $V_L \simeq I$ and corresponds to $\sum_i m_i \lesssim 125$ meV.

6.4. Lower bound on θ_{13}

From the general expression Eq. (49) for the $K_{i\alpha}$, one obtains the following expression for $K_{1\mu}$ for $\rho \simeq \pm\pi/2$ and $m_1 \simeq m_2$,

$$K_{1\mu} \simeq \frac{c_{13}^2\, |s_{12}\, c_{12}\, c_{23}\, m_1\, (1 \pm i) + m_3\, s_{13}\, s_{23}|^2}{m_\star\, |m_1 + m_3\, s_{13}^2|}\,. \tag{82}$$

It is easy to see that, for $s_{13}^2 = 0$, the condition $K_{1\mu} \gtrsim 10$ (for $N_{B/3-L_\mu}^{\text{p}} \simeq 10^{-3}$) would imply $m_1 \gtrsim 30$ meV, clearly incompatible with the upper bound $m_1 \lesssim 20\,\text{meV}$ just obtained. However, for $s_{13}^2 \gtrsim 0.1$, corresponding to $\theta_{13} \gtrsim 5^\circ$, one can simultaneously satisfy $K_{1\mu} \gtrsim 10$ and $m_1 \lesssim 20$ meV. This is an interesting feature of the ST solution, since it predicts a non-vanishing reactor mixing angle [21] as now firmly established by the experimental results.

It should be noticed that this lower bound on θ_{13} strengthens the lower bound Eq. (56) derived from the condition $K_{1\tau} \gtrsim 1$.

6.5. Dirac phase in the fourth quadrant

As we discussed in Section 5.4.2, for τ_A solutions the Dirac phase is driven toward negative values because of its link with the phase σ inside $K_{1\tau}$ that requires, for non-vanishing θ_{13}, $2\sigma - \delta \simeq 0$. In addition there is a subdominant solution for $\delta \simeq \pi$. When the ST condition is imposed this conclusion is strengthened even more by the more stringent lower bound on θ_{13}. The last panel of Fig. 9, where we plotted δ vs. θ_{23} for the experimental allowed 3σ range for θ_{13}, clearly shows this situation. It also shows how δ is basically constrained in the fourth quadrant for θ_{23} in the first octant and $\theta_{23} \gtrsim 38^\circ$. We have just seen how the ST condition necessarily requires θ_{23} in the first octant as a result of the lower bound on m_1. Combining this result with the 3σ lower bound $\theta_{23} \gtrsim 38^\circ$, we conclude that the only way for the ST condition to be satisfied for such high values of θ_{23} is to have δ in the fourth quadrant ($-\pi/2 \lesssim \delta \lesssim 0$). This is an interesting result in light of the experimental hint for $\sin\delta < 0$. The ST condition more definitely requires also $\cos\delta > 0$. From Fig. 5 panel showing δ vs. θ_{23}, it can be seen how, for $N^{\rm p,i}_{B-L} = 10^{-3}$, the highest value of θ_{23} is obtained for $\delta \simeq -60^\circ$ and is given by $\theta_{23} \simeq 41^\circ$ (light blue points for $V_L = I$). This upper bound relaxes to $\theta_{23} \lesssim 43^\circ$ going beyond the approximation $V_L \simeq I$.

7. Inverted ordering

In this section we finally extend the discussion to the case of IO. The expressions (25), (28) and (22) still apply while the asymptotic limits for $m_1 \to 0$ (cf. Eqs. (83)) become now

$$
\begin{aligned}
M_1 &\simeq \frac{m_{D1}^2}{m_{\rm atm}\, c_{12}^2 |c_{13}^2\, e^{2\,i\,\rho} + s_{12}^2|} \approx \frac{m_{D1}^2}{m_{\rm atm}\, c_{12}^2\, c_{13}^2}\,,\\
M_2 &\simeq \frac{m_{D2}^2\, |c_{13}^2\, e^{2\,i\,\rho} + s_{12}^2|}{m_{\rm atm}\, c_{23}^2\, c_{13}^2} \approx \frac{m_{D2}^2\, c_{12}^2}{m_{\rm atm}\, c_{23}^2}\,,\\
M_3 &\simeq \frac{m_{D3}^2}{m_1}\, c_{23}^2\, c_{13}^2\,.
\end{aligned}
\tag{83}
$$

At the same time also Eq. (31) for the RH neutrino mixing matrix, Eq. (41) for the $\varepsilon_{2\alpha}$, Eq. (49) for the $K_{i\alpha}$ and, finally, Eq. (53) for the final asymmetry are also still valid. All the differences arise only when the neutrino masses and the leptonic mixing entries are specified, since these are different from the NO case.

7.1. Successful leptogenesis

As done for NO, we have verified that Eq. (53) is able to reproduce the numerical results of [19] for $V_L = I$ when the condition of successful leptogenesis is imposed. In particular it is confirmed that IO is only marginally allowed, requiring quite a restricted range of values m_1 between 20 and 40 meV and the existence this time of a lower bound on the atmospheric neutrino mixing angle $\theta_{23} \gtrsim 48^\circ$, that therefore has to lie in the second octant. Moreover the lower bound on α_2 is very stringent, and values $\alpha_2 \lesssim 4.5$ are not allowed.

It is interesting to show analytically the origin of some of the differences between IO and NO. The usual starting point is the calculation of $K_{1\tau}$ that this time is particularly simple since we

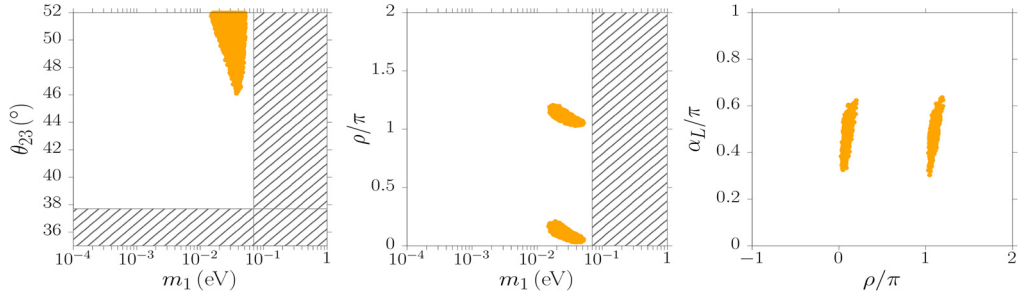

Fig. 10. IO case. Scatter plots for θ_{23} vs. m_1 (left), ρ vs. m_1 (centre) and α_L vs. ρ (right).

can use the approximation $m_2 \simeq m_3$. In this way it is easy to show that $K_{1\tau}$ is minimised for $\rho = n\,\pi$ and in this case one has

$$K_{1\tau} \gtrsim \frac{m_1^2\, s_{13}^2\, c_{23}^2}{m_\star\, m_2}\,, \tag{84}$$

so that the condition $K_{1\tau} \lesssim 1$ simply leads to the upper bound

$$m_1 \lesssim 0.1\ \text{eV}\ \frac{0.01}{s_{13}^2\, c_{23}^2}\,. \tag{85}$$

As we will notice, however, the exact condition $\rho = n\,\pi$ would imply $\sin\alpha_L \simeq 0$ and, therefore, a small (positive) displacement from $\rho = n\,\pi$ is necessary for the asymmetry not to vanish (see central plot in Fig. 10) and clearly this implies that the upper bound is more stringent. In the scatter plot (see left panel in Fig. 10) it is indeed found $m_1 \lesssim 50$ meV. We can also easily estimate the wash-out at the production, calculating

$$K_{2\tau} \simeq \frac{m_3}{m_\star}\, s_{23}^2\,, \tag{86}$$

entering the efficiency factor $\kappa(K_{2\tau}) \simeq 0.5/K_{2\tau}^{1.2}$. We can then calculate the different terms entering the *CP* asymmetry $\varepsilon_{2\tau}$ in the approximation $m_2 \simeq m_{\rm atm}$, $m_1 \ll m_{\rm atm}$ and $\rho = n\,\pi$ finding

$$m_{ee} \simeq m_2\,, \qquad |(m_\nu^{-1})_{\tau\tau}| \simeq \frac{c_{23}^2}{m_1}\,, \qquad |(m_\nu^{-1})_{\mu\tau}| \simeq \frac{s_{23}\, c_{23}}{m_1}\,. \tag{87}$$

In this way we arrive to

$$\varepsilon_{2\tau} \simeq \frac{3}{16\,\pi}\, \frac{\alpha_2^2\, m_c^2}{v^2}\, \frac{s_{23}^2}{c_{23}^4}\, \frac{m_1}{m_{\rm atm}}\, \sin\alpha_L\,. \tag{88}$$

Finally for the effective leptogenesis phase we find

$$\sin\alpha_L \simeq \sin(2\rho - \text{Arg}[\text{c}_{12}^2\, \text{e}^{2\,\text{i}\,\rho} + \text{s}_{12}^2])\,, \tag{89}$$

showing that the phase ρ needs to deviate from $n\,\pi$ for the asymmetry not to vanish and for this reason the upper bound Eq. (85) becomes more stringent.

Combining all terms together, and imposing the successful leptogenesis condition one arrives to a lower bound on m_1 depending on θ_{23},

$$m_1 \gtrsim 32\,\pi\ 10^{-8}\, \frac{m_{\rm atm}\, v^2}{\alpha^2\, m_c^2}\, \frac{c_{23}^4}{s_{23}^2}\, [\kappa(K_{2\tau})]^{-1}\ \sin\alpha_L^{-1}\,. \tag{90}$$

When this lower bound is combined with the upper bound Eq. (85) one finds a lower bound $\theta_{23} \gtrsim 45^\circ$ for $\sin\alpha_L \simeq 0.5$ (the phase cannot be maximal otherwise the condition $K_{1\tau} \lesssim 1$ would be hardly violated: see right panel in Fig. 10) fairly reproducing the results from the scatter plots (see Fig. 10).

7.2. Strong thermal leptogenesis

It is quite straightforward to understand why the ST condition cannot be satisfied in the IO case. Even though the N_1 wash-out of the electron pre-existing component is strong since again one has $K_{1e} = m_{ee}/m_\star \simeq m_2/m_\star \gtrsim 50$, on the other hand the wash-out of the muonic component is very weak since one has

$$K_{1\mu} \simeq \frac{|(m_\nu)_{e\mu}|^2}{m_\star m_{ee}} \simeq \frac{|m_1 s_{13} s_{23} e^{i(2\sigma-\delta)} + c_{12} s_{12} c_{23} (m_3 - m_2)|^2}{m_\star m_2}$$
$$\simeq \frac{m_1^2}{m_\star m_2} s_{13}^2 s_{23}^2 \simeq 0.5\,. \tag{91}$$

This happens because for IO one has $m_2 \simeq m_3$ in a way that there is an almost exact cancellation of the two terms $\propto m_2, m_3$ (those not suppressed by s_{13}^2). This is again, as for NO, a particular example of what happens more generally, beyond $SO(10)$-inspired models, for IO: the wash-out of a muonic pre-existing asymmetry is weakened by this cancellation and produces a lower bound on m_1 [22]. In the case of $SO(10)$-inspired models the cancellation is basically almost exact in a way that the lower bound becomes incompatible with the CMB upper bound and one can conclude that ST $SO(10)$-inspired leptogenesis is simply not viable for IO neutrino masses.

8. Theoretical approximations and uncertainties

Eq. (53) constrains all low energy neutrino parameters to lie on a hypersurface in the low energy neutrino parameter space. However, there are different effects of different nature to be considered that make in a way that this hypersurface is actually a layer with some thickness: the experimental errors on the low energy neutrino parameters; the theoretical uncertainties in the calculation; accounting for deviations from $V_L = I$ introduces a dependence on the parameters of the V_L that since are not measured lead to an intrinsic indetermination within $SO(10)$-inspired models. Of course within a specific model one is able to specify the parameters in the V_L and in this case one can expect and calculate specifically the deviation from the hypersurface described by Eq. (53).

8.1. Beyond the approximation $V_L \simeq I$

In Fig. 5 we have included the results of a scatter plot, for $\alpha = 5$ and NO, of points respecting successful leptogenesis for $I \leq V_L \leq V_{CKM}$ (yellow points), confirming once more previous results [19,22]. When these are compared with the results obtained for $V_L = I$ (the orange points), one can see that there are constraints that do not get strongly modified (e.g. the lower bound on m_1) and constraints that are more greatly modified (e.g. the upper bound on m_1). The most remarkable difference can be noticed in the panel θ_{23} vs. m_1 where a complete new region at large values $m_1 \gtrsim m_{\rm sol}$ appears. This is now mostly excluded by the CMB upper bound on m_1. This region is due to the appearance of a muon-type solution that is possible since when deviations of

V_L from unity are taken into account the strong hierarchy in the CP asymmetries (cf. Eq. (42)) gets much milder and a muonic solution becomes possible [19].

Another clear difference is that for type τ_B solution the upper bound on θ_{23} is much more relaxed. On the other hand the constraints for the type τ_A solution do not change dramatically, except for the well known effect that now there is no lower bound on θ_{13}.

We have also compared the results obtained in the approximation $V_L = I$ (light blue points) and for $I \leq V_L \leq V_{CKM}$ (dark blue points) in the case of ST. One can see how the constraints get moderately relaxed. The lower bound on θ_{13} gets relaxed from $\theta_{13} \gtrsim 5^\circ$ to $\theta_{13} \gtrsim 2^\circ$. The upper bound on θ_{23} gets relaxed from $\theta_{23} \lesssim 41.5^\circ$ to $\theta_{23} \lesssim 43^\circ$, probably the most important effect in light of the current experimental constraints on θ_{23} that tend to favour $\theta_{23} \gtrsim 40^\circ$ at least at 2σ. One can see how the lower bound on m_{ee} gets greatly relaxed.

In Fig. 4 we have plotted of η_B vs. m_1 for three examples where $V_L \neq I$ comparing them to the three examples for $V_L = I$. In all three cases the low energy neutrino parameters are unchanged. One can see how turning on angles and phases in the V_L can significantly enhance the asymmetry, though not dramatically (approximately up to a factor 2).

8.2. Theoretical uncertainties

A detailed discussion of the theoretical uncertainties can be found in [22]. Here we just remind that the main sources of corrections to our results should come by inclusion of flavour coupling and (in the case of the muonic solution) of phantom terms [43]; account of decoherence for $M_2 \gtrsim 10^{11}$ GeV within a density matrix formalism [45–47,39,48]. Minor effects should come from the running of neutrino parameters [49] and a full relativistic calculation of the wash-out rates [50].

9. Summary

We have seen how $SO(10)$-inspired models motivate an interesting scenario of high energy scale leptogenesis with hierarchical RH neutrinos able to reproduce the correct asymmetry when the production from the decays of the next-to-lightest RH neutrinos is taken into account. This scenario implies constraints on the low energy neutrino parameters that will be partially testable with low energy neutrino experiments. In the approximation of negligible misalignment between the Yukawa basis and the charged lepton basis ($V_L = I$), we found a very accurate analytical expression that links all low energy neutrino parameters in quite a non-trivial way. Constraints on each individual parameter depend on the experimental information on the other parameters and interesting predictions can gradually emerge with more experimental information. For example, we have seen how the discovery of a non-vanishing θ_{13} seems to produce combined constraints on the Dirac phase, the atmospheric mixing angle and the absolute neutrino mass scale. This potential interesting feature should, however, be confirmed relaxing the approximation $V_L = I$.

In addition, quite interestingly, for a subset of the successful leptogenesis solutions, $SO(10)$-inspired leptogenesis realises the ST condition, in a way that a large pre-existing asymmetry is efficiently washed-out and the final asymmetry is independent of the initial conditions. This produces very tight constraints on the low energy neutrino parameters characterising the ST $SO(10)$-inspired solution whose predictions will be (almost) completely tested during next years. For example, the discovery of a IO neutrino mass spectrum would certainly rule out the solution like also a value of the atmospheric angle in the second octant. Vice-versa a discovery of NO and atmospheric neutrino mixing angle in the first octant should certainly be regarded as a strong

support to the solution. In this respect it is interesting that some of the current global analyses [23,24] mildly support either IO and θ_{23} in the second octant or NO and θ_{23} in the first octant: in the first case the solution would be undoubtedly ruled out, while the second case should be regarded as a very successful test.

It is also interesting that the experimental value of the reactor mixing angle falls just within quite a narrow range of values allowed by the solution. Interestingly the solution, within the allowed current range for the atmospheric mixing angle, is also potentially able to explain the emerging hint for a negative value of $\sin\delta$, and therefore of J_{CP}, with the additional prediction $\cos\delta > 0$, with $\delta \sim -\pi/4$. We managed to provide a full analytical description of these constraints. In particular we showed why non-vanishing values of the reactor mixing angle are required. Very importantly the ST leptogenesis condition also forces m_1 to lie within a narrow range about $m_1 \simeq 20$ meV. This narrow range necessarily implies the atmospheric angle θ_{23} in the first octant and this explains indirectly why δ has to lie in the fourth quadrant.

The NOνA long baseline experiment [51] is currently taking data and, combined with the results from the other neutrino oscillation experiments, in particular T2K constraints on δ [52] and θ_{13} determination [20], will allow in the next years to test in quite a significant way the predictions on the leptonic mixing matrix unknowns from the ST $SO(10)$-inspired solution. At the same time cosmological observations are starting to corner quasi-degenerate neutrino and might in a close future start to test the narrow window, 75 meV $\lesssim \sum m_i \lesssim$ 125 meV, required by the solution corresponding to semi-hierarchical NO neutrino masses. In longer terms neutrinoless double beta decay experiments should also be able to test the range of values predicted by the solution for m_{ee} centred about $m_{ee} \simeq 15$ meV. In this way one would just miss a further experimental complementary constraint on the Majorana phases for a complete test of the solution (explaining why the solution can 'almost' completely be tested). It is then quite exciting that with $SO(10)$-inspired leptogenesis one has a well motivated opportunity to probe at the same time not only leptogenesis and the see-saw mechanism, but also the $SO(10)$-inspired conditions, shedding light on the model for the origin of neutrino masses and mixing.

Acknowledgements

We wish to thank Ferruccio Feruglio and Steve King for many useful discussions. P.D.B. acknowledges financial support from the NExT/SEPnet Institute, from the STFC Rolling Grant ST/L000296/1 and from the EU FP7 ITN INVISIBLES (Marie Curie Actions, PITN-GA-2011-289442). P.D.B. also wishes to thank the CERN theory group, NORDITA, CP3-Odense and MITP Institutes for the hospitality during the preparation of the work. M.R.F. acknowledges financial support from the STAG Institute. L.M. acknowledges the European Social Fund for supporting his work under the grant MJD387.

Appendix A

In this appendix we provide details on the derivation of the approximate expression (Eq. (31)) for the off-diagonal entries of the RH neutrino mixing matrix U_R. More precisely here we are calculating what we called $\widetilde{U}_R$ while the matrix D_Φ can be calculated using the equation given in the body text though we will omit the tilde to simplify the notation. From the unitarity conditions, $U_{Rik}\, U^\star_{Rjk} = \delta_{ij}$, one finds, for $(i, j) = (1, 2)$ and $(i, j) = (2, 3)$ respectively,

$$U_{R12} \simeq -U^\star_{R21} \quad \text{and} \quad U_{R32} \simeq -U^\star_{R23}\,, \tag{A.1}$$

having neglected respectively $U_{R13}\,U^{\star}_{R23}$ and $U_{R21}\,U^{\star}_{R31}$. On the other hand one has

$$U^{\star}_{R31} \simeq -U_{R13} - U_{R12}\,U^{\star}_{R32}\,, \tag{A.2}$$

since the second term in the RH side is also $\propto m_{D1}/m_{D3}$ and cannot be neglected in this case.

From Eq. (24) we can write $D_M^{-1} \simeq -U_R^{\dagger}\,D_{m_D}^{-1}\,m_\nu\,D_{m_D}^{-1}\,U_R^{\star}$ and, therefore, for the matrix elements we can write

$$\frac{\delta_{ij}}{M_i} \simeq -U^{\star}_{Rki}\,(D_{m_D}^{-1}\,m_\nu\,D_{m_D}^{-1})_{kl}\,U^{\star}_{Rlj}\,. \tag{A.3}$$

For $(i,\,j) = (1,2)$ it is quite straightforward to find

$$U_{R21} \simeq \frac{m_{D1}}{m_{D2}}\,\frac{m_{ve\mu}}{m_{vee}}\,, \tag{A.4}$$

that plugged into Eq. (A.3) for $(i,\,j) = (3,1)$ gives, with the help of Eq. (A.2) and the second Eq. (A.1),

$$U_{R31} \simeq \frac{m_{D1}}{m_{D3}}\,\frac{m_{ve\tau}}{m_{vee}}\,. \tag{A.5}$$

From Eq. (A.3) for $(i,\,j) = 2,3$ and using Eq. (A.1) to write $U^{\star}_{R23}$ in terms of $U^{\star}_{R13}$ and U_{R31} one finds

$$U_{R13} \simeq \frac{m_{D1}}{m_{D3}}\,\frac{(m_\nu^{-1})^{\star}_{e\tau}}{(m_\nu^{-1})^{\star}_{\tau\tau}}\,. \tag{A.6}$$

Finally, from the second equation in (A.1) and Eq. (A.2), one can write

$$U_{R23} \simeq \frac{U_{R13} + U^{\star}_{R31}}{U_{R12}} \simeq \frac{m_{D2}}{m_{D3}}\,\frac{(m_\nu^{-1})^{\star}_{\mu\tau}}{(m_\nu^{-1})^{\star}_{\tau\tau}}\,, \tag{A.7}$$

leading to Eq. (31). In writing these equations we have made use of the fact that the entries of the inverse neutrino mass matrix are related to the entries of the neutrino mass matrix by

$$m_\nu^{-1} = \frac{1}{\det(m_\nu)} \times \begin{pmatrix} m_{\nu\mu\mu}\,m_{\nu\tau\tau} - (m_{\nu\mu\tau})^2 & m_{\nu\mu\tau}\,m_{ve\tau} - m_{ve\mu}\,m_{\nu\tau\tau} & m_{ve\mu}\,m_{\nu\mu\tau} - m_{\nu\mu\mu}\,m_{ve\tau} \\ m_{\nu\mu\tau}\,m_{ve\tau} - m_{ve\mu}\,m_{\nu\tau\tau} & m_{vee}\,m_{\nu\tau\tau} - (m_{ve\tau})^2 & m_{ve\tau}\,m_{ve\mu} - m_{vee}\,m_{\nu\mu\tau} \\ m_{ve\mu}\,m_{\nu\mu\tau} - m_{\nu\mu\mu}\,m_{ve\tau} & m_{ve\mu}\,m_{ve\tau} - m_{vee}\,m_{\nu\mu\tau} & m_{vee}\,m_{\nu\mu\mu} - (m_{ve\mu})^2 \end{pmatrix}. \tag{A.8}$$

The orthogonal matrix entries are given by Eq. (33). Using Eq. (31) and that $(m_\nu\,U^{\star})_{ei} = -(U\,D_m)_{ei}$ one arrives to Eq. (34).

References

[1] P. Ade, et al., Planck Collaboration, Astron. Astrophys. (2014), arXiv:1303.5076.
[2] M. Fukugita, T. Yanagida, Phys. Lett. B 174 (1986) 45.
[3] P. Minkowski, Phys. Lett. B 67 (1977) 421;
T. Yanagida, Conf. Proc. C7902131 (1979) 95;
M. Gell-Mann, P. Ramond, R. Slansky, Conf. Proc. C790927 (1979) 315, arXiv:1306.4669;
S. Glashow, NATO Sci. Ser. B 59 (1980) 687;
R. Barbieri, D.V. Nanopoulos, G. Morchio, F. Strocchi, Phys. Lett. B 90 (1980) 91;
R.N. Mohapatra, G. Senjanovic, Phys. Rev. Lett. 44 (1980) 912.

[4] M.J. Mortonson, U. Seljak, arXiv:1405.5857, 2014;
R. Flauger, J.C. Hill, D.N. Spergel, arXiv:1405.7351, 2014;
R. Adam, et al., Planck Collaboration, arXiv:1409.5738, 2014.
[5] P. Ade, et al., BICEP2 Collaboration, arXiv:1403.3985, 2014.
[6] S. Davidson, A. Ibarra, Phys. Lett. B 535 (2002) 25;
W. Buchmuller, P. Di Bari, M. Plumacher, Nucl. Phys. B 643 (2002) 367.
[7] S. Blanchet, P. Di Bari, J. Cosmol. Astropart. Phys. 0703 (2007) 018, arXiv:hep-ph/0607330.
[8] M. Yoshimura, Phys. Rev. Lett. 41 (1978) 281.
[9] E. Bertuzzo, P. Di Bari, L. Marzola, Nucl. Phys. B 849 (2011) 521, arXiv:1007.1641.
[10] P. Bhupal Dev, P. Millington, A. Pilaftsis, D. Teresi, Nucl. Phys. B 886 (2014) 569, arXiv:1404.1003;
P.S.B. Dev, P. Millington, A. Pilaftsis, D. Teresi, arXiv:1409.8263, 2014.
[11] R. Barbieri, P. Creminelli, A. Strumia, N. Tetradis, Nucl. Phys. B 575 (2000) 61, arXiv:hep-ph/9911315.
[12] E. Nardi, Y. Nir, E. Roulet, J. Racker, J. High Energy Phys. 0601 (2006) 164, arXiv:hep-ph/0601084;
A. Abada, S. Davidson, F.-X. Josse-Michaux, M. Losada, A. Riotto, J. Cosmol. Astropart. Phys. 0604 (2006) 004, arXiv:hep-ph/0601083.
[13] G. Engelhard, Y. Grossman, E. Nardi, Y. Nir, Phys. Rev. Lett. 99 (2007) 081802, arXiv:hep-ph/0612187.
[14] W. Buchmuller, M. Plumacher, Phys. Lett. B 389 (1996) 73, arXiv:hep-ph/9608308;
E. Nezri, J. Orloff, J. High Energy Phys. 0304 (2003) 020, arXiv:hep-ph/0004227;
F. Buccella, D. Falcone, F. Tramontano, Phys. Lett. B 524 (2002) 241, arXiv:hep-ph/0108172.
[15] G. Branco, R. Gonzalez Felipe, F. Joaquim, M. Rebelo, Nucl. Phys. B 640 (2002) 202, arXiv:hep-ph/0202030.
[16] E.K. Akhmedov, M. Frigerio, A.Y. Smirnov, J. High Energy Phys. 0309 (2003) 021, arXiv:hep-ph/0305322.
[17] P. Di Bari, L. Marzola, Nucl. Phys. B 877 (2013) 719, arXiv:1308.1107.
[18] P. Di Bari, A. Riotto, Phys. Lett. B 671 (2009) 462, arXiv:0809.2285.
[19] P. Di Bari, A. Riotto, J. Cosmol. Astropart. Phys. 1104 (2011) 037, arXiv:1012.2343.
[20] K. Abe, et al., T2K Collaboration, Phys. Rev. Lett. 107 (2011) 041801, arXiv:1106.2822;
F. An, et al., DAYA-BAY Collaboration, Phys. Rev. Lett. 108 (2012) 171803, arXiv:1203.1669;
J. Ahn, et al., RENO Collaboration, Phys. Rev. Lett. 108 (2012) 191802, arXiv:1204.0626.
[21] P. Di Bari, L. Marzola, Talks at the DESY Theory Workshop, 2011, http://th-workshop2011.desy.de/.
[22] P. Di Bari, S. King, M. Re Fiorentin, J. Cosmol. Astropart. Phys. 1403 (2014) 050, arXiv:1401.6185.
[23] F. Capozzi, G. Fogli, E. Lisi, A. Marrone, D. Montanino, et al., arXiv:1312.2878, 2013.
[24] M. Gonzalez-Garcia, M. Maltoni, T. Schwetz, arXiv:1409.5439, 2014.
[25] D. Forero, M. Tortola, J. Valle, arXiv:1405.7540, 2014.
[26] X.-G. He, S.S. Law, R.R. Volkas, Phys. Rev. D 78 (2008) 113001, arXiv:0810.1104.
[27] F. Feruglio, K.M. Patel, D. Vicino, J. High Energy Phys. 1409 (2014) 095, arXiv:1407.2913.
[28] S.F. King, J. High Energy Phys. 1401 (2014) 119, arXiv:1311.3295.
[29] S.F. King, J. High Energy Phys. 1408 (2014) 130, arXiv:1406.7005 [hep-ph].
[30] R.N. Mohapatra, G. Senjanovic, Phys. Rev. D 23 (1981) 165;
G. Lazarides, Q. Shafi, C. Wetterich, Nucl. Phys. B 181 (1981) 287.
[31] H. Goh, R. Mohapatra, S.-P. Ng, Phys. Rev. D 68 (2003) 115008, arXiv:hep-ph/0308197;
A. Abada, P. Hosteins, F.-X. Josse-Michaux, S. Lavignac, Nucl. Phys. B 809 (2009) 183, arXiv:0808.2058.
[32] A. Dueck, W. Rodejohann, J. High Energy Phys. 1309 (2013) 024, arXiv:1306.4468 [hep-ph].
[33] P. Di Bari, arXiv:hep-ph/0406115;
S. Blanchet, D. Marfatia, A. Mustafayev, J. High Energy Phys. 1011 (2010) 038, arXiv:1006.2857 [hep-ph].
[34] X.-d. Ji, Y.-c. Li, R. Mohapatra, S. Nasri, Y. Zhang, Phys. Lett. B 651 (2007) 195, arXiv:hep-ph/0605088;
F. Buccella, D. Falcone, C.S. Fong, E. Nardi, G. Ricciardi, Phys. Rev. D 86 (2012) 035012, arXiv:1203.0829;
G. Altarelli, D. Meloni, J. High Energy Phys. 1308 (2013) 021, arXiv:1305.1001.
[35] P. Di Bari, Nucl. Phys. B 727 (2005) 318, arXiv:hep-ph/0502082.
[36] O. Vives, Phys. Rev. D 73 (2006) 073006, arXiv:hep-ph/0512160.
[37] S. Blanchet, P. Di Bari, Nucl. Phys. B 807 (2009) 155, arXiv:0807.0743.
[38] S. Blanchet, P. Di Bari, J. Cosmol. Astropart. Phys. 0606 (2006) 023, arXiv:hep-ph/0603107.
[39] S. Blanchet, P. Di Bari, D.A. Jones, L. Marzola, J. Cosmol. Astropart. Phys. 1301 (2013) 041.
[40] H. Fusaoka, Y. Koide, Phys. Rev. D 57 (1998) 3986, arXiv:hep-ph/9712201.
[41] J. Casas, A. Ibarra, Nucl. Phys. B 618 (2001) 171, arXiv:hep-ph/0103065.
[42] P.H. Chankowski, K. Turzynski, Phys. Lett. B 570 (2003) 198, arXiv:hep-ph/0306059.
[43] S. Antusch, P. Di Bari, D.A. Jones, S.F. King, Nucl. Phys. B 856 (2012) 180.
[44] L. Covi, E. Roulet, F. Vissani, Phys. Lett. B 384 (1996) 169, arXiv:hep-ph/9605319.

[45] S. Blanchet, P. Di Bari, G. Raffelt, J. Cosmol. Astropart. Phys. 0703 (2007) 012, arXiv:hep-ph/0611337.
[46] A. De Simone, A. Riotto, J. Cosmol. Astropart. Phys. 0702 (2007) 005, arXiv:hep-ph/0611357.
[47] M. Beneke, B. Garbrecht, C. Fidler, M. Herranen, P. Schwaller, Nucl. Phys. B 843 (2011) 177, arXiv:1007.4783.
[48] B. Garbrecht, F. Glowna, P. Schwaller, Nucl. Phys. B 877 (2013) 1, arXiv:1303.5498.
[49] S. Antusch, J. Kersten, M. Lindner, M. Ratz, M.A. Schmidt, J. High Energy Phys. 0503 (2005) 024, arXiv:hep-ph/0501272.
[50] D. Boedeker, M. Woermann, J. Cosmol. Astropart. Phys. 1402 (2014) 016, arXiv:1311.2593.
[51] R. Patterson, NOvA Collaboration, Nucl. Phys. B, Proc. Suppl. 235–236 (2013) 151.
[52] K. Abe, et al., T2K Collaboration, Phys. Rev. Lett. 112 (2014) 061802, arXiv:1311.4750.